DOI: 10.1002/ejic.200601207

Broadening the Scope of Ancillary Phosphane-Type Ligands: A Systematic Comparison of PR_3, $PR_2BH_3^-$, and SiR_3^- and Their Chalcogen Derivatives

Theresa I. Kückmann,[a] Franz Dornhaus,[a] Michael Bolte,[a] Hans-Wolfram Lerner,[a] Max C. Holthausen,*[a] and Matthias Wagner*[a]

Keywords: Isoelectronic analogs / P ligands / Si ligands / Ligand design / Boron

This work describes a systematic experimental and theoretical study of the properties of two series of isoelectronic and largely isosteric ligands, namely PPh_2Me, $PPh_2BH_3^-$, and $SiPh_2Me^-$ and $SPtBu_3$, $SPtBu_2BH_3^-$, and $SSitBu_3^-$. In addition, we have also investigated the oxo derivatives $OPPh_2BH_3^-$ and $OSiPh_2Me^-$. Based on X-ray crystal structure determinations (Fe–CO and C–O bond lengths) as well as NMR [e.g. $\delta(^{13}CO)$] and IR [ν(CO)] spectroscopic investigations of the corresponding $[CpFe(CO)_2]^+$ complexes, we can conclude that, with respect to electron donor strength, phosphanyl borohydrides occupy an intermediate position between phosphanes (weakest donors) and silyl ligands (strongest donors). The same is true for the thio derivatives, although the differences are smaller. In the reaction with $[CpFe(CO)_2]^+$, the oxo derivative $OPPh_2BH_3^-$ transfers a hydride ion rather than forming a stable $[CpFe(CO)_2(OPPh_2BH_3)]$ complex. The tendency to undergo hydride-transfer reactions was studied by density functional calculations for the series $PtBu_2BH_3^-$, $OPtBu_2BH_3^-$, and $SPtBu_2BH_3^-$. The results reveal that $OPtBu_2BH_3^-$ is the strongest and $SPtBu_2BH_3^-$ the weakest hydride donor, in accordance with the experimental observations. Theoretical analysis indicates that the three derivatives PPh_2Me, $PPh_2BH_3^-$, and $SiPh_2Me^-$ are truly isolobal species despite variations in their charge distributions.

Introduction

The performance of a homogeneous catalyst depends critically on the steric and electronic properties of its ligands.[1,2] Intense research has therefore been devoted to the development of donor molecules specifically designed for the assembly of a particular catalyst with a well-defined purpose. As a result, homogeneous catalysis with transition-metal complexes has enjoyed enormous success, and catalyst research continues to gain momentum.[3] A wealth of information has been gathered on numerous individual ligand classes, which now must be compared in order to establish their relationship to one another. The goal is to create versatile toolboxes of ligands with smoothly varying donor properties so that the most suitable derivative can easily be selected for the rational de novo design of efficient catalysts.

We have a long-standing interest in the development of boron-based N-donor ligand systems [e.g. mono- and ditopic bis- and tris(pyrazol-1-yl)borates] for applications both in materials science and catalysis.[4–10] In order to extend the range of accessible complexes, we are presently broadening our focus to include negatively charged boron-based P-donor ligands and their isoelectronic silyl analogs. The purpose of this paper is to reveal the underlying relationship between two representatives of these ligand classes, namely phosphanyl borohydrides $PR_2BH_3^-$ and triorganylsilanides SiR_3^-, and to compare them with the well established phosphane ligands PR_3.

A generic methyldiorganylphosphane **A** is shown in Figure 1. On moving to the phosphanyl borohydride **B**, the phosphane methyl group is replaced by a BH_3 moiety. This leaves the central atom unchanged but results in a negatively charged ligand. The substitution pattern is conserved in the corresponding silyl compound **C** but the central phosphorus atom is replaced by silicon, which again introduces a negative charge. The same relationship holds true for the chalcogen derivatives of these compounds (**D**–**F**; Figure 1), which have been the subject of two recent studies.[11,12] We are interested in investigating the similarities as well as the fundamental differences between these three related species. We commence with a brief review of selected literature relevant to this pursuit.

Phosphanes are ubiquitous ligands in coordination chemistry due to their σ-donating and π-accepting properties.[13,14] The degree to which these σ and π components influence the overall coordination characteristics of a given phosphane depends on the phosphorus-bound substituents. The π-acceptor strength of PF_3, for example, is comparable to that of CO, which is often considered the archetypical π-

[a] Institut für Anorganische Chemie, Johann Wolfgang Goethe-Universität Frankfurt am Main,
Max-von-Laue-Straße 7, 60438 Frankfurt, Germany
Fax: +49-69-798-29260
E-mail: Matthias.Wagner@chemie.uni-frankfurt.de
Supporting information for this article is available on the WWW under http://www.eurjic.org or from the author.

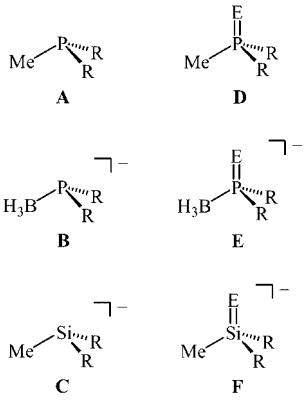

Figure 1. Isoelectronic phosphanes, phosphanyl borohydrides, and silanides, and their chalcogen derivatives.

acceptor ligand. Trialkylphosphanes, on the other hand, are primarily σ-donors and participate to only a small degree in π-backbonding.

Transition metal complexes with silyl ligands, while not as widespread as phosphane complexes, have also received significant attention in the literature.[15,16] Such studies have focused primarily on the reactivity of the Si–M bond, for example in transition-metal-catalyzed hydrosilylation or C–Si bond formation.[15,17] Recently, silyl derivatives have also generated increasing interest as ancillary ligands.[18] Indeed, it has been suggested that silyl ligands might enhance the performance of soluble catalytic systems for hydrogenation or hydroformylation reactions.[19] Silyl ligands are strongly electron-releasing with comparatively poor π-accepting properties and display a pronounced *trans* effect, which makes them potentially complementary ligands to phosphanes.[18,20–22] It is clear, however, that the properties of formally isoelectronic silyl and phosphane ligands differ significantly and that this difference is too large to be considered a gradual transition.

Phosphanyl borohydrides $PR_2BH_3^-$ are intermediate species in which the donor phosphorus atom remains as in phosphanes, but which contain a negative charge, as do silyl ligands. To date, these anionic phosphane analogues have mainly been generated in situ and used as building blocks for the preparation of chiral organophosphanes.[23–26] However, there is a growing number of phosphanyl borohydride transition metal complexes in the literature. Manners et al., for example, have exploited the regioselective insertion of the $Pt(PEt_3)_2$ fragment into the P–H bond of $PPhBH_3(H)_2$ or $PPh_2BH_3(H)$ in order to prepare the platinum phosphanyl borohydride complexes *trans*-[PtH(PPhRBH$_3$)-$(PEt_3)_2$] (R = H, Ph).[27] Other examples of structurally characterized phosphanyl borohydride complexes include the compounds $[(dppp)Pd(C_6F_5)(PPh_2BH_3)]$[28] and $[(C_5Me_5)Fe(CO)_2(PPh_2BH_3)]$.[29] In a 1996 paper, Fu and co-workers described diphenylphosphidoboratabenzene, $PPh_2(BC_5H_5)^-$, as the anionic analog of triphenylphosphane and investigated its coordination chemistry.[30]

While not as common as the parent phosphanes, phosphane oxides also play an important role as ancillary ligands in coordination chemistry,[13] especially in the form of bidentate bisphosphane monooxides [P(O)–P] or P(O)–O and P(O)–N type ligands, which form part of efficient catalytic systems for rhodium- and cobalt-catalyzed hydroformylation reactions.[31–33]

Transition metal siloxide complexes have also been investigated.[34–38] For example, rhodium siloxides are active in catalytic hydrosilylation reactions,[34,39] and titanium, niobium, and tantalum siloxide systems have been used to investigate C–H activation[37] and olefin-to-alkylidene rearrangement.[38]

The corresponding chalcogen derivatives of phosphanyl borohydrides, $EPR_2BH_3^-$ (E = O–Te), have only recently been reported in the literature,[12] and their application as ligands for transition metals has yet to be explored.

In order to shed more light on the relative importance of donor atom and electronic structure for the ligand properties of phosphanes, phosphanyl borohydrides, and silanides, we have investigated two series of isoelectronic, isosteric compounds (Figure 2). In the case of the non-chalcogen species, the diphenyl derivatives **1**, **2a**, and **3a** were chosen for detailed study. In order to still be able to evaluate the effect of increased steric demand, P*t*Bu$_2$BH$_3^-$ (**2b**) was also investigated. For the chalcogen derivatives, both the phenyl and *tert*-butyl systems **4**–**8** were studied.

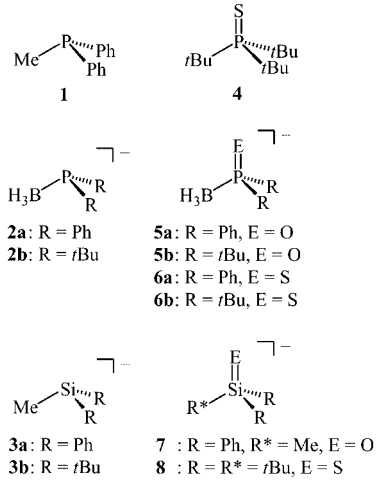

Figure 2. Ligand numbering scheme for isoelectronic species **1**–**3** and **4**–**8**.

For the transition metal site, we chose the cyclopentadienidoiron dicarbonyl fragment $[CpFe(CO)_2]^+$ (in future referred to as Fp^+) as a model system. This fragment is an ideal candidate for our pursuit because it has a single vacant coordination site (often occupied by halides or donor solvent molecules in its isolable derivatives) and all of the ligands in question can be expected to coordinate to it in a similar fashion, regardless of whether the result is a neutral or cationic complex. In addition, its electronic properties can be related to the carbonyl IR stretching frequencies[40] as well as to the ^{13}C NMR shifts of the carbonyl[41] and cyclopentadienido[42] carbon atoms.

Terminal, unbridged phosphane complexes of the Fp^+ fragment are well known in the literature, with one of two synthetic routes generally being applied. The first involves treating Fp^+ complexes containing labile ligands such as thf or I^- with phosphanes.[43–46] In the second, Fp_2 is oxidized in the presence of phosphane ligand, typically with ferrocenium or cobaltocenium ions.[47–49] Using a different approach, Malisch has succeeded in isolating $[(C_5Me_5)Fe(CO)_2(PPh_2Me)]I$, which was prepared by reaction of the corresponding diphenylphosphido complex with MeI and characterized spectroscopically.[29]

To the best of our knowledge, no structurally characterized monomeric $FpSiR_3$ complexes in which the silyl ligand bears only alkyl and/or aryl substituents R have been previously reported. Nevertheless, there are a number of silyl complexes with known molecular structures where the silicon atom is bound to electron-withdrawing functional groups.[50–53] Complexes of Fp^+ bearing silyl ligands with solely aryl and/or alkyl substituents have, however, been spectroscopically characterized and are typically obtained by treating NaFp with a triorganylsilyl chloride.[54–57]

The σ-donor properties of the phosphanyl borohydride **2a** (Figure 2) towards selected main group Lewis acids have already been explored.[58] It was found that **2a** forms stronger Lewis acid–base adducts than the related phosphane PPh_2Me (**1**). Transition metal complexes of phosphanyl borohydrides are rare in the literature, with only a handful of structurally characterized complexes {e.g. $[FpPPh_2(BC_5H_5)]$ and $[(C_5Me_5)Fe(CO)_2(PPh_2BH_3)]$}.[27–30] The complex $[FpPPh_2BH_3]$ was prepared from $FpPPh_2$ and BH_3·thf and was characterized spectroscopically.[59]

The few examples of Fp-phosphane chalcogenide complexes with trialkyl- and triarylphosphane chalcogenides EPR_3 (R = *i*Pr, *t*Bu, Ph; E = O, S, Se) were prepared by reaction with $[Fp(thf)]BF_4$ and characterized spectroscopically[60] and, in part, by cyclic voltammetry.[61] The same synthetic route can be followed for silyl thiolates, and a small number of complexes of the type $FpSSiR_3$ have been isolated.[62] The coordination of chalcogenated phosphanyl borohydrides to the Fp^+ fragment has not been described previously.

Results and Discussion

Synthesis

In order to conduct a detailed comparison of transition metal complexes of the non-chalcogen ligands, compounds $[FpPPh_2Me]I$ (**11I**), $[FpPPh_2BH_3]$ (**12a**), $[FpPtBu_2BH_3]$ (**12b**), and $[FpSiPh_2Me]$ (**13**) were synthesized (Scheme 1). Compound **11I** was prepared from FpI (**9**), $LiPPh_2$, and MeI in thf. Reports of the synthesis of this complex directly from FpI and PPh_2Me (**1**) describe impurities due to the CO-substitution product $[CpFe(CO)(PPh_2Me)I]$.[63] In contrast, the procedure followed here produces the product as a yellow solid in high purity and good yield. Complex **11I** is, however, sensitive to light, and photochemical decomposition can be observed, which proceeds more quickly in solution than in the solid state. When the solid is stored under inert atmosphere and protected from light, the compound is stable for several months. X-ray quality crystals can be obtained by gas-phase diffusion of diethyl ether into an acetonitrile solution of the complex.

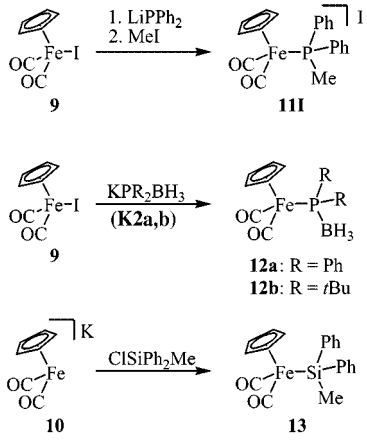

Scheme 1. Complexes of a phosphane and its isoelectronic analogues, **11I**–**13**.

Preparation of the phosphanyl borohydride homologue **12a** in an analogous reaction using BH_3·thf instead of MeI has been reported.[59] However, the general utility of phosphanyl borohydrides as ligands can best be achieved if it is possible to form metal complexes by introducing the preformed ligands, rather than assembling them with the phosphorus atom connected to a metal fragment. With this goal in mind, FpI was treated with $KPPh_2BH_3$ (**K2a**) in thf, which resulted in nearly quantitative formation of the desired compound **12a**. It also proved possible to synthesize $[FpPtBu_2BH_3]$ (**12b**) by the same method. Both complexes were isolated as X-ray quality crystals by gas-phase diffusion of pentane into a concentrated toluene solution of **12a** or **12b**. The yellow solids can be handled in air for short periods of time but decompose upon longer exposure.

Considering the similarities between silanides and phosphanyl borohydrides, it would be desirable to apply the same synthetic route used for complexes of the latter to the preparation of complexes of the former. The sodium silanides $NaSiPh_2Me$[64] (**Na3a**) and $NaSitBu_2Me$[65] (**Na3b**) are both known in the literature, although the former has been characterized only by boiling point determination of the corresponding silane after hydrolysis. The di-*tert*-butyl species **Na3b** is well documented, but the synthesis of the donor-free compound as described by Sekiguchi, which involves reduction of the bromosilane with elemental sodium in boiling heptane, results in a significant amount of disilane impurity.[65] Another common synthesis of sterically hindered sodium silanides, in this case donor-supported, involves the reduction of the corresponding bromosilanes with sodium metal in thf.[66] Biphenyl can be used as a redox catalyst to allow lower reaction temperatures. In an effort to avoid unnecessary and unwanted by-products, this method was used to prepare $(thf)_xNaSitBu_2Me$. The NMR

chemical shifts (^{1}H, ^{13}C, ^{29}Si) of the sodium silanide produced by this route were in good agreement with the published values. Slight variations can be attributed to the fact that the procedure reported here results in a donor-supported silanide, while the literature describes the synthesis of the donor-free compound. Unfortunately, this synthetic method led to unexpected side products. In an attempt to grow crystals of the silanide, dark green blocks of the silylated biphenyl radical [(18-crown-6)(thf)$_2$Na][4,4′-(Si*t*Bu$_2$Me)$_2$(C$_6$H$_4$)$_2$] were isolated.[67] In light of this result and the poor characterization of NaSiPh$_2$Me in the literature, no further attempts to synthesize [FpSiR$_2$Me] (R = Ph, *t*Bu) from Fp$^+$ and SiR$_2$Me$^-$ were undertaken.

As described above, a number of [FpSiR$_3$] complexes have been reported in the literature. Due to the low electronegativity of silicon, these reactions generally proceed with silyl chlorides. This, in essence, represents the umpolung of the procedure used with phosphanyl borohydrides **2a** and **2b**. The synthesis of [FpSiPh$_2$Me] (**13**) by this method has been described.[57] When KFp (**10**) is treated with ClSiPh$_2$Me in thf, the desired complex is formed in nearly quantitative yield (Scheme 1). Impurities can be removed by filtration through silica gel using hexane/CH$_2$Cl$_2$ (2:1) as the eluent. Recrystallization from hexane at –25 °C yields the complex as light-brown plates.

Considering the success achieved with the parent compounds, it was logical to explore the behavior of the chalcogen derivatives KOPPh$_2$BH$_3$ (**K5a**), NaOSiPh$_2$Me (**Na7**), and KSPPh$_2$BH$_3$ (**K6a**) with the Fp$^+$ fragment (the silyl thiolate NaSSiPh$_2$Me is not readily accessible).

When FpI was treated with **K5a** in thf, a colorless solid was slowly deposited over the course of several days. NMR analysis of the resulting mixture revealed conversion of FpI to Fp$_2$ and the appearance of unidentified components in the ^{31}P and ^{11}B NMR spectra. Upon closer inspection of the hydride region of the ^{1}H NMR spectrum, a small amount of FpH[68] could be identified, which is known to be an unstable intermediate that decomposes to Fp$_2$ and H$_2$.[69,70] This finding suggests that rather than forming an Fe–O bond, the iron atom interacts with the borohydride moiety of the ligand, ultimately resulting in hydride transfer. Although the fate of the ligand after hydride transfer remains unclear, it seems likely that oligomeric or polymeric compounds of the type [OPPh$_2$BH$_2$]$_n$ are formed.

The observation of a hydride-transfer product with **K5a** is particularly interesting in light of a comparison with the siloxide **Na7**, since it is unlikely that the methyl moiety would engage in the same kind of behavior. However, when a thf solution of FpI is treated with **Na7**, Fp$_2$ is the only Cp-containing product. In the ^{29}Si NMR spectrum, O(SiPh$_2$Me)$_2$ can be identified as the major silicon-containing product (its ^{1}H, ^{13}C, and ^{29}Si NMR shifts correspond to an authentic sample prepared from ClSiPh$_2$Me and NaOSiPh$_2$Me).[71–73] A similar reaction to that with FpI was observed when the alternative starting material [Fp(thf)]PF$_6$ was treated with **K5a** and **Na7**. However, in the latter case a significant amount of ferrocene was formed in addition to Fp$_2$.

The reaction of KSPPh$_2$BH$_3$ (**K6a**) with [Fp(thf)]PF$_6$ (**14PF$_6$**) was more successful. Thus, when the reactants were combined in CH$_2$Cl$_2$ at –78 °C and warmed to room temperature overnight, a colorless precipitate (KPF$_6$) formed. Changing the solvent to toluene with subsequent filtration through a plug of silica gel on a frit allowed the product complex [FpSPPh$_2$BH$_3$] (**16a**, Scheme 2) to be isolated as an orange oil. Although the NMR and IR data clearly indicate the formation of the complex, attempts to obtain single crystals of **16a** failed.

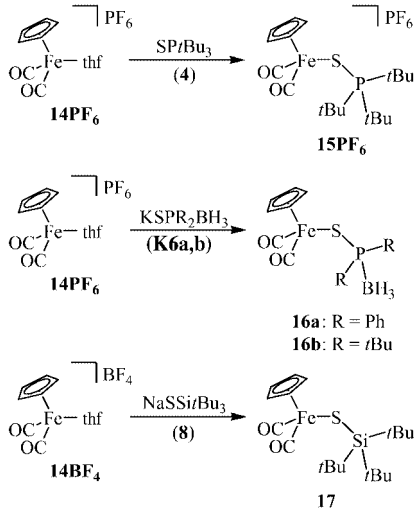

Scheme 2. Complexes of a phosphane sulfide and its isoelectronic analogs, **15PF$_6$**–**17**.

In the hope of isolating a crystalline product, the same reaction was carried out using the *tert*-butyl derivative **K6b** rather than the phenyl derivative **K6a**. In this case, filtration of the crude product through silica gel and recrystallization from benzene yielded orange X-ray quality needles of [FpSP*t*Bu$_2$BH$_3$] (**16b**).

Since the isosteric silyl thiolate NaSSi*t*Bu$_2$Me is not easily accessible, we turned to the sterically more hindered NaSSi*t*Bu$_3$ (**Na8**). This compound reacts readily with [Fp(thf)]BF$_4$ (**14BF$_4$**) in CH$_2$Cl$_2$ at room temperature to give the desired complex [FpSSi*t*Bu$_3$] (**17**; Scheme 2). Recrystallization from a concentrated pentane solution yielded X-ray quality crystals.

The complex of the analogous phosphane sulfide **4**, [FpSP*t*Bu$_3$]BF$_4$ (**15BF$_4$**), has been described in the literature.[60] Using the PF$_6^-$ salt **14PF$_6$**, we were able to isolate X-ray quality crystals of the compound by gas-phase diffusion of pentane into a solution of [FpSP*t*Bu$_3$]PF$_6$ (**15PF$_6$**) in CHCl$_3$ (Scheme 2).

It was thus possible to prepare two series of three isoelectronic compounds each in which all six compounds were characterized by X-ray crystal structure analysis and NMR and IR spectroscopy. Complexes **11I**, **12a**, and **13** are derived from the phosphane PPh$_2$Me, while complexes **15PF$_6$**, **16b**, and **17** are related to the phosphane sulfide SP*t*Bu$_3$. A comparison of these two sets of isoelectronic complexes grants insight into the electronic differences between the ligands.

Structural and Spectroscopic Comparison of 11I, 12a, 12b, and 13

Selected bond lengths and angles for **11I**, **12a**, **12b**, and **13** are compiled in Table 1. Details of the X-ray crystal structure analyses of these compounds are summarized in Table 5.

Table 1. Selected bond lengths [Å] for compounds **11I**–**13**; calculated values in italics.

	Fe–P/Si	Fe–CO (av.)	C–O (av.)
11I	2.236(2)	1.779(9)	1.146(10)
calc.	*2.338*	*1.787*	*1.158*
12a	2.2705(6)	1.772(2)	1.141(2)
calc.	*2.367*	*1.772*	*1.163*
12b	2.3404(6)	1.756(3)	1.142(3)
13	2.3353(5)	1.755(2)	1.160(3)
calc.	*2.389*	*1.757*	*1.168*

Phosphane compound **11I** crystallizes in the triclinic space group $P\bar{1}$ with well-separated complex cations and iodide anions (Figure 3). The Fe–P bond [2.236(2) Å] is in the range of Fe–P distances found for other $[FpPR_3]^+$ complex cations.[74]

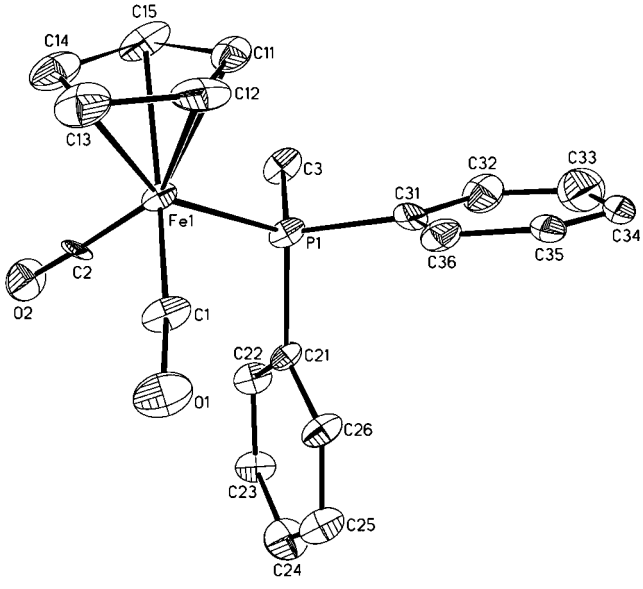

Figure 3. Solid-state structure of the complex cation of **11I**. Thermal ellipsoids are drawn at the 50% probability level. H atoms have been omitted for clarity.

Both phosphanyl borohydride complexes **12a** and **12b** crystallize in the orthorhombic space group $P2_12_12_1$ (Figures 4 and 5, respectively). Their structural parameters are similar, although **12b** shows signs of the higher steric demand of the *tert*-butyl substituents: the Fe–P bond [2.3404(6) Å] is somewhat longer than in the diphenyl derivative **12a** [2.2705(6) Å]. The Fe–CO bonds, on the other hand, are slightly shorter in **12b** (Table 1). Furthermore, the B–P–Fe–COG torsion angles (COG = center of gravity of the Cp ring) differ significantly: the torsion angle is 56.8° for **12a** and –175.9° for **12b**. The only other structurally characterized Fp complex with an anionic phosphorus/boron ligand was reported by Fu and co-workers and contains coordinated diphenylphosphidoboratabenzene.[30] This complex has an Fe–P bond of 2.276(2) Å, which is similar to that in **12a** [2.2705(6) Å]. The Fe–CO distances in Fu's compound [av. 1.742(10) Å] are slightly shorter than in **12a** [av. 1.772(2) Å] but similar to those in **12b** [av. 1.756(3) Å]. The C–O distances [av. 1.169(9) Å] are longer than in both of the phosphanyl borohydride complexes [**12a**: av. 1.141(2) Å; **12b**: av. 1.142(3) Å].

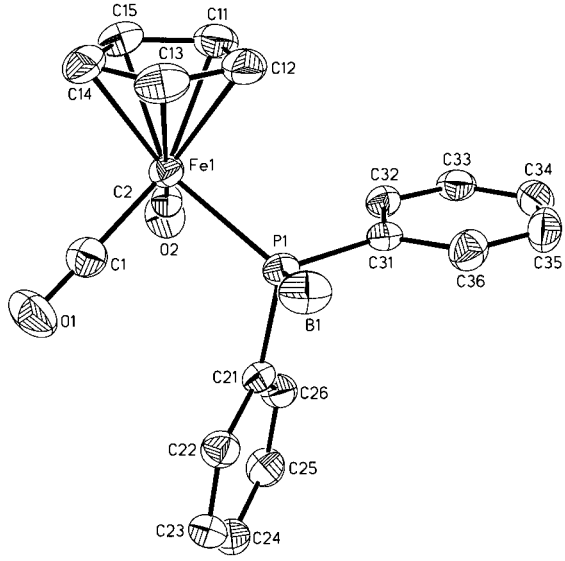

Figure 4. Solid-state structure of **12a**. Ellipsoids are drawn at the 50% probability level. H atoms have been omitted for clarity.

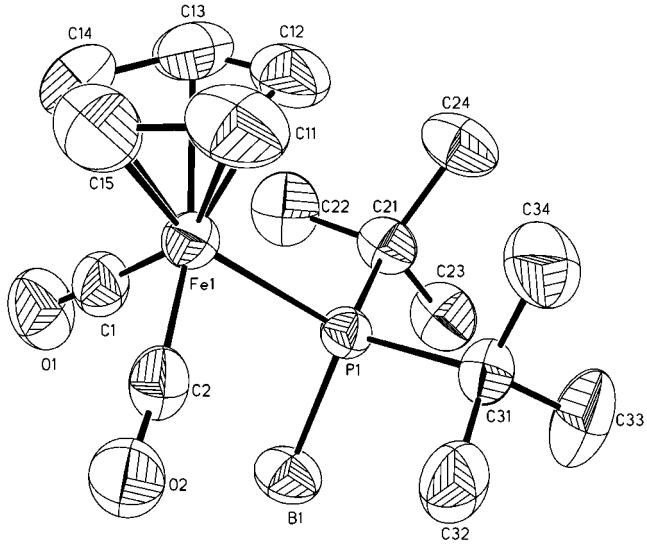

Figure 5. Solid-state structure of **12b**. Ellipsoids are drawn at the 50% probability level. H atoms have been omitted for clarity.

Complex **13** (orthorhombic, $P2_12_12_1$; Figure 6) has the longest Fe–Si bond [2.3353(5) Å] of the structurally characterized Fp-silyl complexes in the literature, with the exception of those complexes with donor silicon atoms bound to silyl residues without electron-withdrawing substituents (cf. $[FpSiMe_2SiPh_3]$: Fe–Si = 2.346(1) Å;[75] $[FpSiPh(SiMe_3)_2]$: Fe–Si = 2.366(1) and 2.355(1) Å in two crystallographically independent molecules[76]). The Fe–Si bond in **13** cannot, of course, be compared directly to the Fe–P bonds in complexes **11I**, **12a**, and **12b**. However, the difference between the Fe–P bond length in **12a** and the Fe–Si bond length in **13** is roughly equivalent to the difference in the covalent radii[71] of P and Si. The Fe–CO distances in **13** are comparable to those found in other Fp-silyl complexes[74] but shorter than those in complexes **11I** and **12a** (Table 1). The C–O bonds found in silyl complex **13** [av. 1.160(3) Å] are roughly 0.015 Å longer than in the complexes **11I** and **12**. This indicates that the π-backbonding from the iron center to the CO ligands is most pronounced in the silyl complex and suggests that **3a** is the strongest donor of the isoelectronic series **1**, **2a**, and **3a**.

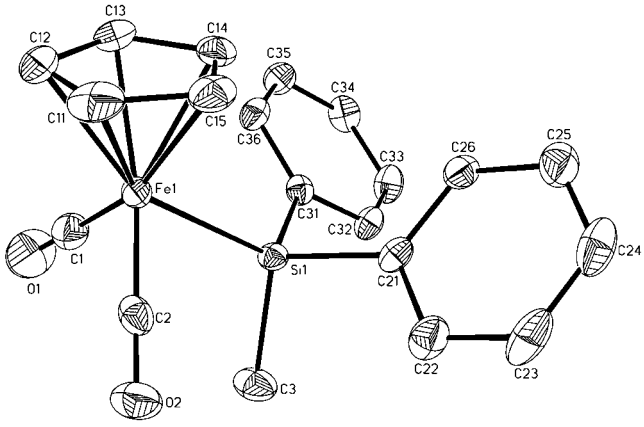

Figure 6. Solid-state structure of **13**. Ellipsoids are drawn at the 50% probability level. H atoms have been omitted for clarity.

This interpretation of relative donor strengths is supported by the ^{13}C NMR chemical shifts of the carbonyl carbon atoms. A summary of spectroscopic data can be found in Table 2. It has been shown in the literature that an increase in the donor capacity of an ancillary ligand in a carbonyl complex leads to a shift of the carbonyl carbon atom resonance to lower field.[41,49,77] The carbonyl carbon atom of silyl complex **13** resonates at δ = 215.8 ppm. The corresponding signals for **12a** and **11I** are found at δ = 213.5 and 210.4 ppm, respectively. The ^{13}C NMR chemical shifts of the cyclopentadienido ligands in metal carbonyl complexes also correlate to the electron density at the metal center, although in this case higher electron density corresponds to a shift to higher field.[42,49,77] Phosphane complex **11I** contains the Cp ring with the most deshielded carbon nuclei (δ = 89.1 ppm). The cyclopentadienido ring of **12a** resonates at δ = 86.8 ppm (**12b**: δ = 86.5 ppm), and the corresponding signal for silyl complex **13** can be seen at δ = 84.4 ppm. In summary, the NMR spectroscopic data also support the conclusion that the following trend can be established for the donor strengths of the isoelectronic, isosteric ligands: **3a** > **2a** > **1**.

In the ^{31}P NMR spectrum, the resonance of the P atom in **12b** is found at δ = 81.4 ppm, a shift to considerably lower field compared to **11I** (δ = 48.6 ppm) and **12a** (δ = 34.3 ppm). This is attributable to the difference in steric demand between the two complexes. This effect has already been observed for potassium phosphanyl borohydrides **K2a** and **K2b**[78] as well as for the parent phosphanes PPh_3 and $PtBu_3$.[79] The $^1J_{P,C}$ coupling constants can be correlated to the degree of s character in the P–C bonding orbital.[79] For the two isosteric compounds **11I** and **12a**, $^1J_{P,C}$ (C-*i*) is significantly larger for the phosphane complex (**11I**: 52.9 Hz; **12a**: 27.8 Hz), thereby indicating a larger degree of s character in the P–C-*i* bonding orbital of **11I**. A similar relationship between the $^1J_{P,C}$ values is observed for the free ligands and can easily be explained by Bent's rule.[58,80]

Comparison of the carbonyl IR stretching frequencies is, of course, also an important measure of donor strength in carbonyl complexes (Table 2). In accordance with the interpretation of the ^{13}C NMR spectra, complex **11I** is found to have the highest CO stretching frequencies (2055 and 2011 cm^{-1} in MeCN solution). These values compare favorably with those found in the literature for similar complexes.[81–83] Introduction of the BH_3 moiety and consequently of a negative charge in **12a** leads to a marked decrease in the frequencies of these vibrations to 2030 and 1982 cm^{-1} (MeCN solution). The relatively low-energy bands found for complex **13** (1994 and 1938 cm^{-1}; MeCN

Table 2. Selected spectroscopic parameters for compounds **11I**–**13**; calculated values in italics.

	$\tilde{\nu}$(CO)[a] [cm^{-1}]	δ(^{13}C) (CO)[b] ($^2J_{P,C}$ [Hz])	δ(^{13}C) (Cp)[b]	δ(^{13}C) (C-*i*)[b] ($^1J_{P,C}$ [Hz])	δ(^{31}P/^{29}Si)[b]
11I	2055, 2011 (2033)	210.4 (24.2)	89.1	134.1 (52.9)	48.6
calc.	*2029*[c]	*205.7*	*89.1*	*128.9*	–
12a	2030, 1982 (2006)	213.5 (18.0)	86.8	140.2 (27.8)	34.3
calc.	*2002*[c]	*208.6*	*88.6*	*139.2*	–
12b	2029, 1982	215.5 (17.0)	86.5	–	81.4
13	1994, 1938 (1966)	215.8	84.4	144.6	35.1
calc.	*1977*[c]	*208.5*	*85.6*	*142.9*	–

[a] In MeCN; ($\tilde{\nu}_{as}$ + $\tilde{\nu}_{s}$)/2 given in parentheses. [b] **11I** in CD_3CN and **12**–**13** in C_6D_6. [c] ($\tilde{\nu}_{as}$ + $\tilde{\nu}_{s}$)/2 scaled by 0.9884 to correct for systematic errors.

Table 3. Selected bond lengths [Å] and angles [°] for compounds **15PF$_6$**, **16b**, and **17**; calculated values in italics.

	Fe–S	S–P/Si	Fe–CO (av.)	C–O (av.)	OC–Fe–CO	Fe–S–P/Si
15PF$_6$	2.3469(4)	2.0473(5)	1.799(2)	1.139(3)	93.35(9)	127.88(2)
calc.	*2.434*	*2.072*	*1.791*	*1.158*	*95.3*	*129.4*
16b	2.3125(8)	2.087(1)	1.784(3)	1.144(4)	98.0(2)	115.86(4)
calc.	*2.399*	*2.104*	*1.784*	*1.159*	*97.0*	*118.6*
17	2.345(2)	2.147(2)	1.776(5)	1.151(6)	93.1(2)	129.01(7)
calc.	*2.387*	*2.194*	*1.774*	*1.162*	*94.6*	*127.9*

solution) are consistent with the NMR spectroscopic data, which indicate that the silyl ligand is the strongest donor of the three.

When moving from **1** to **2a** to **3a** within the Fp^+ system, it is also interesting to consider the effect of exchanging the Cp ligand for Cp* (Cp* = $C_5Me_5^-$) while leaving the other ligands unchanged. While the Cp* silyl complex has not been described in the literature, both the phosphane and phosphanyl borohydride adducts have been reported by Malisch and co-workers.[29] In CH_2Cl_2 solution, the CO stretching frequencies are observed at 2029 and 1987 cm^{-1} for the phosphane complex [Cp*Fe(CO)$_2$(PPh$_2$Me)]I, thereby demonstrating that the effect of exchanging Cp for Cp* is comparable to exchanging the phosphane ligand for the corresponding phosphanyl borohydride. Bands attributable to the CO ligands in [Cp*Fe(CO)$_2$(PPh$_2$BH$_3$)], on the other hand, are found at 2007 and 1959 cm^{-1} (CH_2Cl_2 solution). These frequencies lie above those seen for complex **13**, thus indicating that moving from the phosphanyl borohydride to the silyl ligand has a more dramatic effect on the electronic structure of the compound than replacing Cp with Cp*. Taken together, these results suggest that, when viewed electronically, the difference between the phosphane and phosphanyl borohydride ligands is somewhat smaller than between the phosphanyl borohydride and silyl ligands.

Structural and Spectroscopic Comparison of 15PF$_6$, 16b, and 17

Selected bond lengths and angles for **15PF$_6$**, **16b**, and **17** are compiled in Table 3. Details of the X-ray crystal structure analyses of these compounds are summarized in Table 6.

The three iron–sulfur complexes [FpSP*t*Bu$_3$]PF$_6$ (**15PF$_6$**; orthorhombic, $P2_12_12_1$, Figure 7), [FpSP*t*Bu$_2$BH$_3$] (**16b**; orthorhombic, *Pbca*, Figure 8) and [FpSSi*t*Bu$_3$] (**17**; triclinic, $P\bar{1}$, Figure 9) all adopt the expected structure with monodentate, end-on coordination of the sulfide ligands. Separated ion pairs are found in **15PF$_6$**. The effect of the increased steric bulk of **15PF$_6$** and **17** compared to **16b** is most noticeable in the Fe–S–P/Si bond angle, which is nearly 130° in the tri-*tert*-butyl derivatives **15PF$_6$** [127.88(2)°] and **17** [129.01(7)°], compared to 115.86(4)° in **16b**. The Fe–S bond is also affected by the steric strain: **15PF$_6$** and **17** possess the longest reported Fe–S bonds of all Fp complexes with terminal sulfur ligands [2.3469(4) and 2.345(2) Å, respectively].[74] The less sterically hindered complex **16b**, on the other hand, has an Fe–S bond of 2.3125(8) Å. This complex also displays an OC–Fe–CO angle of 98.0(2)°, nearly 5° larger than those found for the two related complexes with three *t*Bu residues.

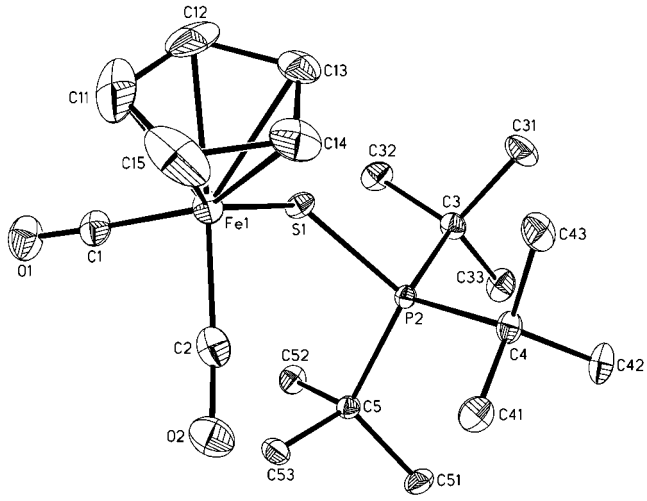

Figure 7. Solid-state structure of the complex cation of **15PF$_6$**. Ellipsoids are drawn at the 50% probability level. H atoms have been omitted for clarity.

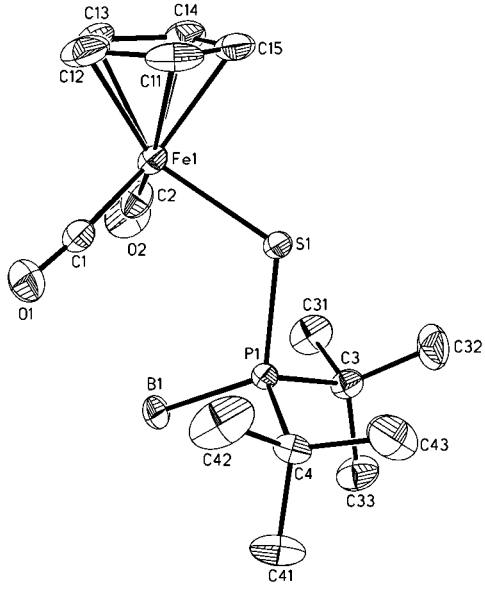

Figure 8. Solid-state structure of **16b**. Ellipsoids are drawn at the 50% probability level. H atoms have been omitted for clarity.

The iron–carbonyl bond lengths and the C–O distances in the carbonyl ligands, however, seem to follow trends that are independent of steric hindrance. Of complexes **15PF$_6$**,

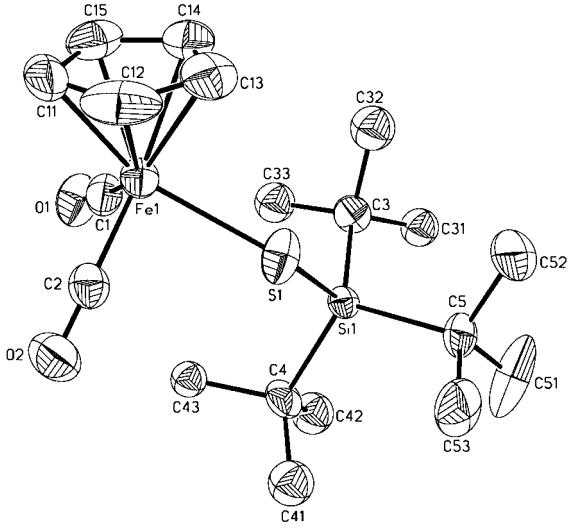

Figure 9. Solid-state structure of **17**. Ellipsoids are drawn at the 50% probability level. H atoms have been omitted for clarity.

16b, and **17**, for example, $[FpSPtBu_3]PF_6$ (**15PF$_6$**) displays the longest Fe–CO and the shortest C–O distances [an average of 1.799(2) and 1.139(3) Å, respectively]. The equally sterically hindered silyl thiolate complex **17**, on the other hand, has the shortest Fe–CO and the longest C–O bond [an average of 1.776(5) and 1.151(6) Å, respectively], although the individual C–O distances for this complex are quite different [1.139(6) and 1.163(6) Å]. The phosphanyl borohydride sulfide complex **16b** displays intermediate average bond lengths of 1.784(3) (Fe–CO) and 1.144(4) Å (C–O). These results indicate that the donor-strength trends observed for the non-chalcogen complexes **11I**–**13** also hold true for the thio derivatives. The silyl thiolate **8** appears to be the strongest donor, causing increased Fe–CO backbonding, which leads to a shortening of the Fe–CO bonds and lengthening of the C–O bonds, followed by **6b** and finally phosphane sulfide **4**.

This general trend is also supported by the chemical shifts of the CO carbon atoms in the ^{13}C NMR spectra (Table 4). As explained above, a more deshielded CO carbon atom correlates to a stronger donor ligand being attached to the same metal center.[41,42,49,77] The silyl thiolate complex **17** has the furthest downfield CO signal (δ = 215.1 ppm), while the carbonyl ligands of **16b** and **15PF$_6$** resonate at δ = 213.1 and 211.5 ppm, respectively (cf. $[FpSSiiPr_3]$: δ = 214.7;[62] $[FpSPPh_3]PF_6$: δ = 211.3 ppm[61]). In contrast to complexes **11I**–**13**, the differences in the chemical shifts of the carbon atoms in the Cp rings of complexes **15PF$_6$**–**17** are too small to discern any meaningful trends.

When considering the IR data (Table 4), silyl thiolate complex **17** is found to have CO vibrations at 2030 and 1982 cm^{-1}, compared to 2040 and 1994 cm^{-1} for **16b** and 2054 and 2010 cm^{-1} for **15BF$_4$**. The steric influence on the IR stretching frequencies appears to be minimal, as $[FpSPPh_2BH_3]$ (**16a**) displays bands at 2042 and 1998 cm^{-1}, which vary only slightly from those of the corresponding *tert*-butyl species **16b**. These results correspond well with published data.[60,62] It can thus be concluded that the CO stretching frequencies in the IR spectra clearly indicate that the silyl thiolate is the strongest donor of the three, while the phosphane sulfide is the weakest.

In summary, X-ray, IR, and NMR spectroscopic data indicate that differences in the electron densities of the non-chalcogen complexes **11I**–**13** on the one hand and the thio complexes **15PF$_6$**–**17** on the other follow the same qualitative trend. However, the differences found for **15PF$_6$**–**17** are less than half as large as those for **11I**–**13**.

Quantum Chemical Calculations

The experimental studies described thus far were augmented by quantum chemical calculations in order to learn more about qualitative differences in the charge density distribution between formally isoelectronic ligands as well as between the $[CpFe(CO)_2]^+$ complexes of these ligands and also about the hydride-donor capacities of phosphanyl borohydrides compared to their chalcogen derivatives. The latter computations were inspired by the experimental observation that the parent phosphanyl borohydride $PtBu_2BH_3^-$ (**2b**) and the corresponding thio derivative **6b** react with the $CpFe(CO)_2$ fragment with formation of a coordinative Fe–P and Fe–S bond, respectively. In contrast, the oxo derivative $OPPh_2BH_3^-$ (**5a**) does not form stable complexes. Instead, we identified the hydride species FpH in the reaction mixture, which is most likely generated by hydride transfer from the BH_3 group.

For the calculation of complex structures and vibrational frequencies, we employed the BP86 functional in combination with the SVP valence double-zeta basis of Ahlrichs and

Table 4. Selected spectroscopic parameters for compounds **15PF$_6$**–**17**; calculated values in italics.[a]

	$\tilde{\nu}$(CO) [cm^{-1}]	δ(^{13}C) (CO) ($^3J_{P,C}$ [Hz])	δ(^{13}C) (Cp)	δ(^{13}C) (*C*Me$_3$) ($^1J_{P,C}$ [Hz])	δ(^{31}P/^{29}Si)
15PF$_6$	2054, 2010[60] (2032)	211.5(2.3)	87.4	44.1(24.4)	93.8
calc.	*2028*[b]	*211.1*	*89.5*	–	–
16a	2042, 1998	212.1(4.4)	86.3	–	48.3
16b	2040, 1994 (2017)	213.1(3.1)	86.5	36.8(20.7)	86.8
calc.	*2022*[b]	*212.6*	*87.5*	–	–
17	2030, 1982 (2006)	215.1	86.9	25.3	29.2[c]
calc.	*2004*[b]	*213.0*	*88.4*	–	–

[a] IR spectra measured in CH_2Cl_2; NMR spectra measured in CD_2Cl_2 unless otherwise noted; ($\tilde{\nu}_{as}$ + $\tilde{\nu}_s$)/2 given in parentheses. [b] ($\tilde{\nu}_{as}$ + $\tilde{\nu}_s$)/2 scaled by 0.9884 to correct for systematic errors. [c] In C_6D_6.

co-workers.[84] The good agreement between computed and experimental values for key geometric data (cf. Tables 1 and 3), as well as for characteristic spectroscopic parameters (cf. Tables 2 and 4) validates this level of density functional theory for an adequate description of electronic structures of the class of compounds studied here.[85,86] For the computation of thermodynamic data for the hypothetical hydride transfer reaction sketched in Scheme 3, we employed the more reliable B3LYP functional in combination with the TZVP valence triple-zeta basis set of Ahlrichs et al.[87] All computations were performed with the Gaussian03 program.[88] Electrostatic potential surfaces were obtained from analogous computations employing the SPARTAN program.[89]

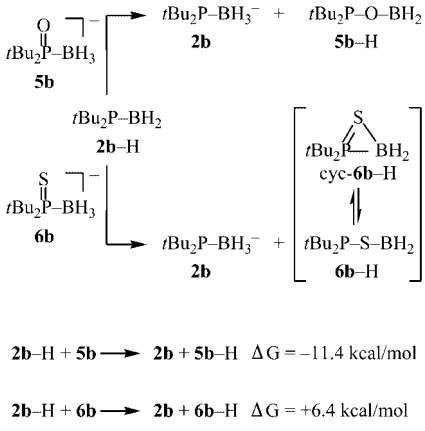

Scheme 3. Isodesmic reactions to assess the relative hydride donor strengths of P*t*Bu$_2$BH$_3^-$ (**2b**), OP*t*Bu$_2$BH$_3^-$ (**5b**), and SP*t*Bu$_2$BH$_3^-$ (**6b**).

An inspection of the electrostatic potential surfaces of PPh$_2$BH$_3^-$ (**2a**) and SiPh$_2$Me$^-$ (**3a**; Figure 10) clearly reveals an accumulation of negative charge concentrated on the BH$_3$ fragment for the phosphanyl borohydride and on the silicon atom for the silyl ligand. In contrast, all of the chalcogen derivatives OP*t*Bu$_2$BH$_3^-$ (**5b**), SP*t*Bu$_2$BH$_3^-$ (**6b**), OSi*t*Bu$_3^-$, and SSi*t*Bu$_3^-$ (**8**) bear the bulk of their negative charge on the chalcogen atom (Figure 10).

Given this qualitative background, it is at first glance surprising to see that **2a** and **2b** react with FpI to give complexes **12a** and **12b**, respectively, whereas treatment of FpI with **5a** leads to hydride transfer and formation of FpH and ultimately of Fp$_2$. The reactivities of **2a/2b** and **5a** with respect to FpI are obviously not governed simply by electrostatic attraction between the positively charged iron center and the most negatively charged part of the ligand molecule; other factors appear to play an important role. We suspected that in the case of ligand **5a**, a neighboring group effect might be responsible for the facile hydride abstraction, because the resulting borane OPPh$_2$BH$_2$ (**5a**-H) can stabilize itself by intramolecular O–B adduct formation leading to a three-membered P–O–B ring. In the case of PR$_2$BH$_2$, the electron deficiency of the boron atom can only be alleviated by P–B pπ–pπ bonding, which is not very efficient.[90]

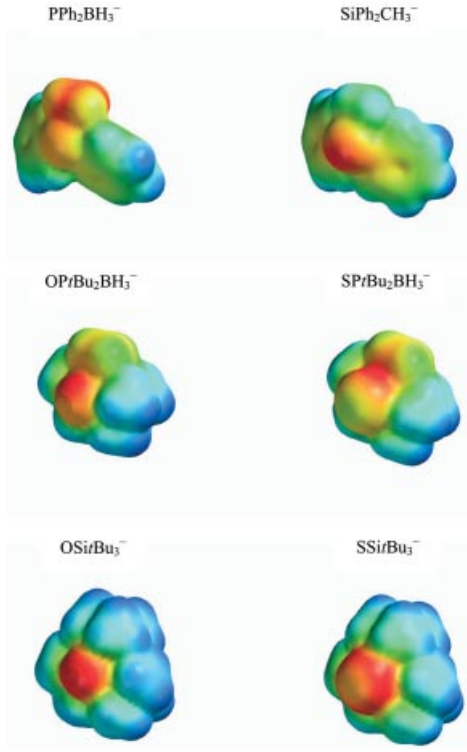

Figure 10. Electrostatic potential surfaces of the anionic ligands PPh$_2$BH$_3^-$ (**2a**), SiPh$_2$Me$^-$ (**3a**), OP*t*Bu$_2$BH$_3^-$ (**5b**), SP*t*Bu$_2$BH$_3^-$ (**6b**), OSi*t*Bu$_3^-$, and SSi*t*Bu$_3^-$ (**8**); color code: red = negative potential; blue = positive potential.

To test the relevance of a possible neighboring group effect, we calculated the molecular structures of the monomeric products of hydride abstraction from P*t*Bu$_2$BH$_3^-$ (**2b**), OP*t*Bu$_2$BH$_3^-$ (**5b**), and SP*t*Bu$_2$BH$_3^-$ (**6b**) (Scheme 3). After geometry optimization, the P–B length in P*t*Bu$_2$BH$_2$ (**2b**-H; 1.818 Å) indicates very little double-bond character between the two atoms. In the case of the oxo derivative OP*t*Bu$_2$BH$_2$, an interesting rearrangement is observed computationally which leads to a migration of the BH$_2$ fragment from phosphorus to oxygen via the anticipated three-membered P–O–B ring (Scheme 3). In the resulting isomer *t*Bu$_2$P–O–BH$_2$ (**5b**-H), pronounced O–B π-bonding aids in the stabilization of the BH$_2$ fragment (O–B = 1.352 Å). To assess the relative stabilities of P*t*Bu$_2$BH$_2$ and *t*Bu$_2$P–O–BH$_2$, we computed the free reaction energy for the isodesmic reaction P*t*Bu$_2$BH$_2$ + OP*t*Bu$_2$BH$_3^-$ → P*t*Bu$_2$BH$_3^-$ + *t*Bu$_2$P–O–BH$_2$ and obtained a value of –11.4 kcal mol^{-1} (Scheme 3). A neighboring group effect similar to the one suggested for hydride-transfer reactions of **5b** may also be operative in the thio derivative **6b**. This in turn raises the question as to why this ligand reacts with [Fp(thf)]$^+$ to form [FpSP*t*Bu$_2$BH$_3$] (**16b**) rather than [FpH]. To address this point, we also calculated the molecular structure of SP*t*Bu$_2$BH$_2$ and found two minima, one containing a three-membered P–S–B ring and the other being the open-chain isomer (Scheme 3). Both isomers are similar in energy, with cyc-**6b**-H being less stable than the open chain species **6b**-H by merely 2.6 kcal mol^{-1}. We interpret this result as fol-

lows: due to poor orbital overlap, S–B π-bonding is less favorable than O–B π-bonding, and consequently S–B σ-donation becomes competitive, even though the resulting cyclic structure suffers from severe Baeyer strain. As before, we computed the free reaction energy for the isodesmic reaction $PtBu_2BH_2 + SPtBu_2BH_3^- \rightarrow PtBu_2BH_3^- + tBu_2P–S–BH_2$ (Scheme 3). Contrary to our results for the O-containing analogs, we found this process to be endergonic by +6.4 kcal mol^{-1} relative to the more stable open-chain isomer. Hence, we conclude that hydride abstraction from $OPtBu_2BH_3^-$ (**5b**) is significantly more facile (by 17.8 kcal mol^{-1}) than from $SPtBu_2BH_3^-$ (**6b**). These theoretical findings agree very well with our experimental observations.

In all three compounds [**11**]$^+$, **12a**, and **13**, the CpFe(CO)$_2$ fragment bears a positive charge q (obtained from NPA analyses) which is largest in the cationic phosphane complex [**11**]$^+$ (q = + 0.486), intermediate in the phosphanyl borohydride complex **12a** [q = +0.302; Δq([**11**]$^+$ – **12a**) = 0.184], and smallest in the silyl complex **13** [q = +0.072; Δq(**12a** – **13**) = 0.230]. This finding supports the conclusion drawn from inspection of the IR and NMR spectroscopic data that silyl ligand **3a** is a significantly stronger electron donor than phosphanyl borohydride ligand **2a**. A similar trend is also visible for the series of complexes [**15**]$^+$ (q = +0.576), **16b** [q = +0.435; Δq([**15**]$^+$ – **16b**) = 0.141], and **17** [q = +0.353; Δq(**16b** – **17**) = 0.082], even though the differences in the computed NPA charges on the three CpFe(CO)$_2$ fragments are less pronounced with a sulfur atom between the iron center and the P/Si atom. Again, these results are nicely reflected by the changes of the CO stretching frequencies: The highest wavenumbers are found for [**15**]$^+$, while a shift to lower wavenumbers is observed for **17** (Table 4), although this difference is much smaller than in the case of [**11**]$^+$ and **13** (Table 2). An inspection of the HOMOs of the three isoelectronic ligands **1**, **2a**, and **3a** reveals very similar topologies, all of which correspond to the lone pair being located on the donor atoms P or Si (Figure 11). This finding provides convincing evidence that the interaction of these ligands with transition metal ions will be of essentially the same nature and implies that these ligands are truly isolobal species. Quantitatively, however, the degree of charge transfer is different for the different ligand classes, with phosphanes being the weakest and silyl ligands being the strongest donors.

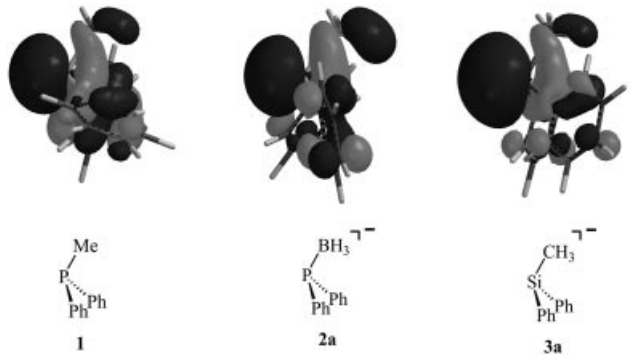

Figure 11. HOMOs of the series of isoelectronic ligands PPh_2Me (**1**), $PPh_2BH_3^-$ (**2a**), and $SiPh_2Me^-$ (**3a**).

Conclusions

A series of isoelectronic and isosteric iron complexes [CpFe(CO)$_2$(EPh$_2$XH$_3$)]$^{n+}$ (E = Si, X = C; E = P, X = C, B; n = 0, 1) **11I**, **12a**, and **13** has been synthesized and characterized by X-ray crystallography and ^{1}H and heteronuclear NMR and IR spectroscopy. A comparison of the structural and spectroscopic properties of compounds **11I**–**13** indicates that the silyl ligand **3a** displays the highest propensity towards electron donation, followed by the anionic phosphanyl borohydride ligand **2a**. The phosphane ligand **1** is the weakest donor.

In addition, the reactivity of phosphane chalcogenides, phosphanyl borohydride chalcogenides, and silyl chalcogenolates with the [CpFe(CO)$_2$]$^+$ fragment has been investigated. A second series of isoelectronic complexes [CpFe(CO)$_2$(SE*t*Bu$_2$XH$_3$)]$^{n+}$ (E = Si, X = C; E = P, X = C, B; n = 0, 1) **15PF$_6$**–**17** has been isolated with *tert*-butyl rather than phenyl residues and fully characterized. The conclusion that the silyl species is the strongest donor of the sulfur-containing ligands can be drawn, but this effect, now mediated by the sulfur atom, is not as pronounced as for the non-chalcogen species **11I**–**13**, and the differences in the CO stretching frequencies in the IR spectra and the ^{13}C NMR resonances of the CO carbon atoms are about half as large in **15PF$_6$**–**17** as in **11I**–**13**. The molecular structures of all crystallographically characterized compounds as well as key spectroscopic parameters have been calculated by DFT. Overall, an excellent agreement was found between experimentally and theoretically derived data. In the reaction with [CpFe(CO)$_2$]$^+$, the oxo derivative $OPPh_2BH_3^-$ transfers a hydride ion rather than forming a stable [CpFe(CO)$_2$(OPPh$_2$BH$_3$)] complex. The tendency to undergo hydride transfer reactions has been studied by DFT calculations for the series $PtBu_2BH_3^-$, $OPtBu_2BH_3^-$, and $SPtBu_2BH_3^-$. The results reveal that $OPtBu_2BH_3^-$ is the strongest and $SPtBu_2BH_3^-$ the weakest hydride donor, in agreement with experimental observations. Further theoretical analysis indicates that the three derivatives PPh_2Me, $PPh_2BH_3^-$, and $SiPh_2Me^-$ are truly isolobal species, despite variations in their charge distributions.

Experimental Section

General Considerations: All reactions and manipulations of air-sensitive compounds were carried out under an atmosphere of dry nitrogen using standard Schlenk techniques. Solvents were freshly distilled under argon from sodium/benzophenone (thf, diethyl ether, toluene, C_6D_6) or sodium-lead alloy (pentane, hexane) prior to use. MeCN, CD_3CN, CH_2Cl_2, CD_2Cl_2, and $CDCl_3$ were dried with molecular sieves (4 Å) and degassed. NMR spectra were recorded with Bruker AMX 250, DPX 250, Avance 300, or Avance 400 spectrometers. ^{1}H and ^{13}C chemical shifts are reported relative to tetramethylsilane and were referenced against residual solvent

peaks (C_6D_5H: δ = 7.16; C_6D_6: δ = 128.06; $CHCl_3$: δ = 7.26; $CDCl_3$: δ = 77.16 ppm).[91] ^{11}B NMR spectra were referenced against external $BF_3{\cdot}OEt_2$. ^{31}P NMR spectra are reported relative to external H_3PO_4 (85%). ^{29}Si NMR spectra were referenced against external TMS and recorded using the INEPT pulse sequence with empirically optimized parameters for polarization transfer from the methyl and phenyl substituents (**13**) or the *t*Bu substituents (**Na3b** and **17**). Abbreviations: Fp = $CpFe(CO)_2$, n.r. = multiplet expected but not resolved. IR spectra were recorded with a Perkin–Elmer 1650 FTIR spectrophotometer or a Jasco FT/IR-420 spectrophotometer. Elemental analyses were performed by the microanalytical laboratory of the J. W. Goethe University, Frankfurt(Main).

Materials: Li, Na, KH, *n*BuLi solution (ca. 1.6 M in hexane), BH_3·thf solution (1 M in thf), PPh_3, $ClSiPh_2Me$, biphenyl, FpI, and MeI were obtained from commercial sources (Aldrich, Fluka, Acros or Chemetall) and used as received. $HPPh_2$ was obtained by reductive cleavage of PPh_3 with Li powder in thf and subsequent hydrolysis and distillation, as described by Bianco and Doronzo.[92] Deprotonation of $HPPh_2$ with *n*BuLi yields $LiPPh_2$;[93] employing hexane leads to precipitation of solvent-free $LiPPh_2$. Bromination of $HSitBu_2Me$[94] according to the literature method[95] yields $BrSitBu_2Me$. KFp (**10**),[96] $KPPh_2BH_3$ (**K2a**),[12,58] and $KPtBu_2BH_3$ (**K2b**)[12,58] were prepared by literature methods. $[Fp(thf)]PF_6$ (**14PF$_6$**) was obtained by treating $[Cp_2Fe]PF_6$ with Fp_2 as reported by Catheline and Astruc.[97] $[Fp(thf)]BF_4$ (**14BF$_4$**) was prepared from FpI and $AgBF_4$.[98]

Synthesis of (thf)$_x$NaSi*t*Bu$_2$Me (Na3b): Na (2.0 g, 87.0 mmol) and biphenyl (1.29 g, 8.4 mmol) were stirred overnight in thf (20 mL) to give a dark green solution surrounding blocks of unreacted sodium. A solution of $BrSitBu_2Me$ (3.38 g, 14.2 mmol) in thf (15 mL) was then added dropwise to this mixture over 2.5 h. After stirring for 16 h, all volatiles were removed in vacuo, and the dark brown residue was extracted with pentane (25 mL). After filtration, the filter cake was washed with pentane (10 mL). Volatiles were removed in vacuo overnight from the dark brown filtrate, and the resulting brown residue was dissolved in thf (30 mL) to give a 0.305 M solution of the product in thf (9.15 mmol, 64%). ^1H NMR (C_6D_6, 250.13 MHz): δ = 0.33 (s, 3 H, $SiCH_3$), 1.35 ppm (s, 18 H, CCH_3). $^{13}C\{^1H\}$ NMR (C_6D_6, 62.90 MHz): δ = 0.3 ($SiCH_3$), 21.3 (CCH_3), 32.2 ppm (s, CCH_3). $^{29}Si\{^1H\}$ NMR (C_6D_6, 49.7 MHz): δ = 14.4 ppm.

Synthesis of [FpPPh$_2$Me]I (11I): A solution of $LiPPh_2$ (0.147 g, 0.77 mmol) in thf (6 mL) was added with stirring to a solution of FpI (**9**, 0.233 g, 0.77 mmol) in thf (8 mL) at –78 °C. Slowly warming to ambient temperature overnight resulted in a color change from black to dark red and the formation of a colorless precipitate (LiI). The mixture was filtered and the filtrate treated with a solution of MeI (0.112 g, 0.79 mmol) in thf (3 mL). The resulting dark yellow precipitate was washed with thf (2 × 5 mL) and dried in vacuo. Yield: 0.243 g (63%). X-ray quality crystals were obtained by gas-phase diffusion of diethyl ether into a solution of **11I** in MeCN. ^1H NMR (CD_3CN, 400.13 MHz): δ = 2.38 (d, $^2J_{P,H}$ = 10.5 Hz, 3 H, CH_3), 5.38 (d, $^3J_{P,H}$ = 1.6 Hz, 5 H, Cp), 7.50–7.64 ppm (m, 10 H, H-*o,m,p*). $^{13}C\{^1H\}$ NMR (CD_3CN, 100.63 MHz): δ = 19.5 (d, $^1J_{P,C}$ = 35.4 Hz, CH_3), 89.1 (d, $^2J_{P,C}$ = 0.5 Hz, Cp), 130.4 (d, $^3J_{P,C}$ = 11.0 Hz, C-*m*), 132.3 (d, $^2J_{P,C}$ = 10.2 Hz, C-*o*), 132.9 (d, $^4J_{P,C}$ = 2.8 Hz, C-*p*), 134.1 (d, $^1J_{P,C}$ = 52.9 Hz, C-*i*), 210.4 ppm (d, $^2J_{P,C}$ = 24.2 Hz, CO). $^{31}P\{^1H\}$ NMR (CD_3CN, 161.98 MHz): δ = 48.6 ppm (s). IR (MeCN): $\tilde{\nu}$ = 2055, 2011 cm^{-1} (CO). $C_{20}H_{18}FeIO_2P$ (504.06): calcd. C 47.65, H 3.60; found C 47.46, H 3.65.

Synthesis of [FpPPh$_2$BH$_3$] (12a): A solution of $KPPh_2BH_3$ (**K2a**; 0.239 g, 1.00 mmol) in thf (10 mL) was added with stirring to a solution of FpI (**9**, 0.304 g, 1.00 mmol) in thf (10 mL) at –78 °C. Slowly warming to ambient temperature overnight resulted in a color change from black to light brown and formation of a colorless precipitate (KI). The mixture was filtered and the solvent removed from the filtrate in vacuo. The resulting brown solid residue was washed with pentane (5 mL) and extracted with toluene (10 mL). The toluene was removed from the filtrate in vacuo to give the product as a yellow crystalline material. Yield: 0.274 g (73%). X-ray quality crystals were obtained by gas-phase diffusion of pentane into a solution of **12a** in toluene. ^1H NMR (C_6D_6, 250.13 MHz): δ = 2.3 (m, 3 H, BH_3), 4.16 (d, $^3J_{P,H}$ = 1.6 Hz, 5 H, Cp), 6.97–7.16 (m, 6 H, H-*m,p*), 7.93–8.02 ppm (m, 4 H, H-*o*). $^{11}B\{^1H\}$ NMR (C_6D_6, 128.37 MHz): δ = –28.0 ppm (d, $^1J_{P,B}$ = 44 Hz). $^{13}C\{^1H\}$ NMR (C_6D_6, 62.90 MHz): δ = 86.8 (n.r., Cp), 128.3 (d, $^3J_{P,C}$ = 8.7 Hz, C-*m*), 129.3 (d, $^4J_{P,C}$ = 2.3 Hz, C-*p*), 133.3 (d, $^2J_{P,C}$ = 8.0 Hz, C-*o*), 140.2 (d, $^1J_{P,C}$ = 27.8 Hz, C-*i*), 213.5 ppm (d, $^2J_{P,C}$ = 18.0 Hz, CO). $^{31}P\{^1H\}$ NMR (C_6D_6, 161.98 MHz): δ = 34.3 ppm (m). IR (MeCN): $\tilde{\nu}$ = 2030, 1982 cm^{-1} (CO). $C_{19}H_{18}BFeO_2P$ (375.96): calcd. C 60.74, H 4.83; found C 60.58, H 4.73.

Synthesis of [FpP*t*Bu$_2$BH$_3$] (12b): A solution of $KPtBu_2BH_3$ (**K2b**, 0.291 g, 1.47 mmol) in thf (10 mL) was added with stirring to a solution of FpI (**9**, 0.446 g, 1.47 mmol) in thf (10 mL) at –78 °C. Slowly warming to ambient temperature overnight resulted in a color change from black to yellow and formation of a colorless precipitate (KI). The mixture was filtered and the solvent removed from the filtrate in vacuo. The resulting brown solid residue was washed with pentane (5 mL) and extracted with toluene (10 mL). The toluene was removed from the filtrate in vacuo to give the product as a yellow crystalline material. Yield: 0.355 g (72%). X-ray quality crystals were obtained by gas-phase diffusion of pentane into a solution of **12b** in toluene. ^1H NMR (C_6D_6, 250.13 MHz): δ = 1.35 (d, $^3J_{P,H}$ = 11.9 Hz, 18 H, CH_3), 1.60 (q, $^1J_{B,H}$ = 93.6 Hz, 3 H, BH_3), 4.33 ppm (s, 5 H, Cp). $^{11}B\{^1H\}$ NMR (C_6D_6, 128.37 MHz): δ = –30.0 ppm (d, $^1J_{P,B}$ = 49 Hz). $^{13}C\{^1H\}$ NMR (C_6D_6, 62.90 MHz): δ = 31.2 (d, $^2J_{P,C}$ = 2.0 Hz, CH_3), 37.4 (d, $^1J_{P,C}$ = 6.6 Hz, CCH_3), 86.5 (n.r., Cp), 215.5 ppm (d, $^2J_{P,C}$ = 17.0 Hz, CO). $^{31}P\{^1H\}$ NMR (C_6D_6, 161.98 MHz): δ = 81.4 ppm (m). IR (MeCN): $\tilde{\nu}$ = 2029, 1982 cm^{-1} (CO). $C_{15}H_{26}BFeO_2P$ (335.99): calcd. C 53.62, H 7.80; found C 53.48, H 7.69.

Synthesis of [FpSiPh$_2$Me] (13): A solution of $ClSiPh_2Me$ (0.33 mL, 0.367 g, 1.57 mmol) in thf (8 mL) was added dropwise to a suspension of KFp (0.307 g, 1.42 mmol) in thf (10 mL). After stirring overnight, volatiles were removed in vacuo, then the brown residue was extracted with pentane (4 × 10 mL) and filtered. Removal of the solvent yielded the crude product as a brown oil (0.392 g, 74%). The crude product was purified by filtration through silica gel under an inert atmosphere using hexane/CH_2Cl_2 (2:1) as the eluent, which yielded the product as a yellow solid after removal of the volatiles in vacuo. X-ray quality crystals were obtained from hexane solution at –25 °C. ^1H NMR (300.0 MHz, C_6D_6): δ = 0.95 (s, 3 H, CH_3), 3.97 (s, 5 H, Cp), 7.21, 7.69 ppm (2 × m, 6 H, 4 H, H-*o,m,p*). $^{13}C\{^1H\}$ NMR (75.4 MHz, C_6D_6): δ = 5.5 (CH_3), 84.4 (s, Cp), 128.0 (C-*m* or C-*o*), 128.4 (s, C-*p*), 134.6 (C-*m* or C-*o*), 144.6 (C-*i*), 215.8 ppm (CO). $^{29}Si\{^1H\}$ NMR (59.6 MHz, C_6D_6): δ = 35.1 ppm. IR (MeCN): $\tilde{\nu}$ = 1994, 1938 cm^{-1} (CO). $C_{20}H_{18}FeO_2Si$ (374.28): calcd. C 64.18, H 4.85; found C 64.14, H 4.88.

Reaction of KOPPh$_2$BH$_3$ (K5a) with FpI (9): An NMR tube was charged with **K5a** (0.05 g, 0.2 mmol), FpI (**9**; 0.06 g, 0.2 mmol), and [D$_8$]thf (0.6 mL), and the tube was flame-sealed and shaken

until all the solids had dissolved. Slow deposition of a colorless precipitate (KI) took place over several days. Analysis by NMR spectroscopy showed slow formation of Fp_2 and several unidentified phosphorus- and boron-containing products. The integrals of the ^1H NMR Cp resonances of Fp_2 and FpI account for over 95% of the total Cp region integral. Main phosphorus-containing product, approx. 60% yield by ^{31}P NMR: $^{31}P\{^1H\}$ NMR ([D$_8$]thf, 161.98 MHz): δ = 80.8 ppm (m); ^{11}B NMR ([D$_8$]thf, 128.37 MHz): δ = –37.5 ppm (m). Analysis of the hydride region of the ^1H NMR spectrum showed small amounts of FpH at δ = –11.7 ppm.[68]

Reaction of $NaOSiPh_2Me$ (Na7) with FpI (9): A Schlenk flask was charged with FpI (**9**; 0.220 g, 0.72 mmol) in thf (5 mL), cooled to –78 °C, and a solution of **Na7** (0.170 g, 0.72 mmol) in thf (5 mL) was added dropwise to this solution. The mixture was then warmed to room temperature overnight. All volatiles were removed in vacuo, and the brown residue was extracted with toluene and filtered. The only major Cp-containing product in the filtrate was Fp_2 and the only major Si-containing product $O(SiPh_2Me)_2$, both of which were identified by comparison with authentic samples. Red crystals of $[(NaOSiPh_2Me)_4(Fp_2)_2]$ were isolated by removing toluene from the filtrate, washing the residue with benzene, and recrystallizing from toluene. It should be noted that the solubility of the adduct is significantly higher in toluene than in benzene. IR $[(NaOSiPh_2Me)_4(Fp_2)_2]$ (KBr): $\tilde{\nu}$ = 2005 (m), 1957 (s), 1932 (m), 1756 (m), 1735 (s) cm^{-1} (CO).

Synthesis of $[FpSPtBu_3]PF_6$ (15PF$_6$): The synthesis and NMR and IR data of the complex cation as its BF_4 salt have been reported by Kuhn and Schumann (data given in Table 4 are for the PF_6 salt).[60] We modified their procedure by using $[Fp(thf)]PF_6$ instead of the BF_4^- salt, as described in the literature.[97] X-ray quality crystals were obtained by gas-phase diffusion of pentane into a solution of **15PF$_6$** in $CHCl_3$. $C_{19}H_{32}F_6FeO_2P_2S$ (556.30): calcd. C 41.02, H 5.80; found C 40.97, H 5.81.

Synthesis of $[FpSPPh_2BH_3]$ (16a): A solution of $KSPPh_2BH_3$ (**K6a**; 0.098 g, 0.36 mmol) in thf (3 mL) was added to a solution of $[Fp(thf)]PF_6$ (**14PF$_6$**; 0.143 g, 0.36 mmol) in CH_2Cl_2 (30 mL) with stirring at –78 °C. As the mixture warmed to ambient temperature overnight, the color lightened from dark red to orange. The solvent was removed in vacuo and the resulting red-brown solid residue washed with pentane (2 × 5 mL) and extracted with toluene (2 × 10 mL). The extracts were filtered through silica gel, and the toluene was removed from the filtrate in vacuo to give the product as an orange oil. Yield: 0.106 g (72%). ^1H NMR (CD_2Cl_2, 300.03 MHz): δ = 1.25 (br. m, 3 H, BH_3), 5.08 (s, 5 H, Cp), 7.1–7.9 ppm (m, 10 H, H-*o,m,p*). $^{11}B\{^1H\}$ NMR (CD_2Cl_2, 96.26 MHz): δ = –33.8 ppm (d, $^1J_{P,B}$ = 55 Hz). $^{13}C\{^1H\}$ NMR (CD_2Cl_2, 75.45 MHz): δ = 86.3 (s, Cp), 128.5 (d, $^3J_{P,C}$ = 9.9 Hz, C-*m*), 130.6 (d, $^4J_{P,C}$ = 2.5 Hz, C-*p*), 132.0 (d, $^2J_{P,C}$ = 9.9 Hz, C-*o*), 136.2 (d, $^1J_{P,C}$ = 46.4 Hz, C-*i*), 212.1 ppm (d, $^3J_{P,C}$ = 4.4 Hz, CO). $^{31}P\{^1H\}$ NMR (CD_2Cl_2, 121.46 MHz): δ = 48.3 ppm (br. m). IR (CH_2Cl_2): $\tilde{\nu}$ = 2042, 1998 cm^{-1} (CO). A correct elemental analysis could not be obtained due to residual solvent and an unidentified impurity that could not be removed.

Synthesis of $[FpSPtBu_2BH_3]$ (16b): A solution of $KSPtBu_2BH_3$ (**K6b**; 0.137 g, 0.60 mmol) in thf (3 mL) was added to a solution of $[Fp(thf)]PF_6$ (**14PF$_6$**; 0.185 g, 0.47 mmol) in CH_2Cl_2 (40 mL) with stirring at –78 °C. As the mixture warmed to ambient temperature overnight, the color lightened from dark red to orange, and a colorless precipitate (KPF_6) formed. The solvent was removed in vacuo and the resulting red-brown semi-solid residue was extracted with pentane (2 × 10 mL). The extracts were filtered through silica gel (approx. 1 cm) on a Schlenk frit. The product adsorbed completely on the silica gel and was subsequently washed with 30 mL of pentane. It was eluted with benzene, and all volatiles were removed in vacuo to give a dark red oil. Upon standing overnight, fine orange needles of **16b** formed in X-ray quality. Yield: 0.100 g (58%). ^1H

Table 5. Crystallographic data for compounds **11I**–**13**.

	11I	**12a**	**12b**	**13**
Empirical formula	$C_{20}H_{18}FeIO_2P$	$C_{19}H_{18}BFeO_2P$	$C_{15}H_{26}BFeO_2P$	$C_{20}H_{18}FeO_2Si$
Formula mass	504.06	375.96	335.99	374.28
Color, shape	orange, block	yellow, block	yellow, block	light-brown, plate
Temperature [K]	173(2)	203(2)	293(2)	173(2)
Crystal system	triclinic	orthorhombic	orthorhombic	orthorhombic
Space group	$P\bar{1}$	$P2_12_12_1$	$P2_12_12_1$	$P2_12_12_1$
a [Å]	9.768(1)	8.488(1)	7.7785(5)	7.2717(6)
b [Å]	12.026(2)	13.727(2)	14.802(1)	15.532(1)
c [Å]	18.416(3)	15.195(2)	14.991(1)	16.055(1)
α [°]	108.78(1)	90	90	90
β [°]	98.99(1)	90	90	90
γ [°]	91.41(1)	90	90	90
V [Å^3]	2016.6(5)	1770.4(4)	1725.9(2)	1813.3(3)
Z	4	4	4	4
$D_{calcd.}$ [g cm^{-3}]	1.660	1.411	1.293	1.371
F(000)	992	776	712	776
μ [mm^{-1}]	2.368	0.949	0.964	0.906
Crystal size [mm]	0.19 × 0.15 × 0.14	0.32 × 0.22 × 0.19	0.48 × 0.45 × 0.34	0.32 × 0.26 × 0.11
Reflections collected	15825	29550	17282	9046
Independent reflns (R_{int})	7125 (0.0792)	3679 (0.0583)	3246 (0.0590)	3321 (0.0292)
Data/restraints/parameters	7125/0/451	3679/0/217	3246/0/182	3321/0/218
GOOF on F^2	1.108	0.857	0.973	1.005
R_1, wR_2 [$I > 2\sigma(I)$]	R_1 = 0.0666, wR_2 = 0.0631	R_1 = 0.0215, wR_2 = 0.0440	R_1 = 0.0270, wR_2 = 0.0650	R_1 = 0.0223 wR_2 = 0.0512
R_1, wR_2 (all data)	R_1 = 0.1274, wR_2 = 0.0684	R_1 = 0.0271, wR_2 = 0.0448	R_1 = 0.0307, wR_2 = 0.0662	R_1 = 0.0259 wR_2 = 0.0522
Largest difference peak/hole [e Å^{-3}]	1.613/–2.791	0.290/–0.150	0.188/–0.162	0.187/–0.195

Table 6. Crystallographic data for compounds **15PF$_6$**, **16b**, and **17**.

	15PF$_6$	**16b**	**17**
Empirical formula	$C_{19}H_{32}F_6FeO_2P_2S$	$C_{15}H_{26}BFeO_2PS$	$C_{19}H_{32}FeO_2SSi$
Formula mass	556.30	368.05	408.45
Color, shape	red, plate	orange, needle	orange, plate
Temperature [K]	173(2)	173(2)	173(2)
Crystal system	orthorhombic	orthorhombic	triclinic
Space group	$P2_12_12_1$	*Pbca*	$P\bar{1}$
a [Å]	8.3294(3)	12.3927(8)	8.671(1)
b [Å]	14.2375(5)	15.1586(8)	8.707(1)
c [Å]	20.7808(9)	19.310(1)	16.215(2)
α [°]	90	90	86.25(1)
β [°]	90	90	88.78(1)
γ [°]	90	90	62.46(1)
V [Å^3]	2464.4(2)	3627.5(4)	1083.0(3)
Z	4	8	2
$D_{calcd.}$ [g cm^{-3}]	1.499	1.348	1.252
F(000)	1152	1552	436
μ [mm^{-1}]	0.885	1.035	0.856
Crystal size [mm]	0.34 × 0.23 × 0.12	0.17 × 0.09 × 0.08	0.18 × 0.15 × 0.08
Reflections collected	45095	31420	10454
Independent reflns (R_{int})	6885 (0.0563)	3330 (0.0622)	3997 (0.0996)
Data/restraints/parameters	6885/0/281	3330/0/191	3997/60/213
GOOF on F^2	1.053	0.934	0.952
R_1, wR_2 [$I > 2\sigma(I)$]	R_1 = 0.0295, wR_2 = 0.0789	R_1 = 0.0397, wR_2 = 0.0742	R_1 = 0.0699, wR_2 = 0.1704
R_1, wR_2 (all data)	R_1 = 0.0303, wR_2 = 0.0794	R_1 = 0.0671, wR_2 = 0.0805	R_1 = 0.0986, wR_2 = 0.1888
Largest difference peak/hole [e Å^{-3}]	0.447/–0.323	0.325/–0.521	0.530/–0.744

NMR (CD_2Cl_2, 300.03 MHz): δ = 0.68 (m, 3 H, BH_3), 1.27 (d, $^3J_{P,H}$ = 13.2 Hz, 18 H, CH_3), 5.12 ppm (s, 5 H, Cp). $^{11}B\{^1H\}$ NMR (CD_2Cl_2, 96.26 MHz): δ = –37.1 ppm (d, $^1J_{P,B}$ = 55 Hz). $^{13}C\{^1H\}$ NMR (CD_2Cl_2, 75.45 MHz): δ = 28.4 (d, $^2J_{P,C}$ = 2.3 Hz, CH_3), 36.8 (d, $^1J_{P,C}$ = 20.7 Hz, *C*CH_3), 86.5 (s, Cp), 213.1 ppm (d, $^3J_{P,C}$ = 3.1 Hz, CO). $^{31}P\{^1H\}$ NMR (CD_2Cl_2, 121.46 MHz): δ = 86.8 ppm (br. m). IR (CH_2Cl_2): $\tilde{\nu}$ = 2040, 1994 cm^{-1} (CO). $C_{15}H_{26}BFeO_2PS$ (368.05): calcd. C 48.95, H 7.12; found C 48.06, H 7.12.

Synthesis of [FpSSi*t*Bu$_3$] (17): Solid $(thf)_2NaSSitBu_3$ (**Na8**, 0.155 g, 0.39 mmol) was added in one portion to a solution of $[Fp(thf)]BF_4$ (**14BF$_4$**; 0.131 g, 0.39 mmol) in CH_2Cl_2 (12 mL). After 4 h stirring, the volatiles were removed from the reaction mixture and the brown residue was extracted with pentane (5 mL) and filtered through Celite® on a frit. The filter cake was then washed with pentane (2 × 5 mL). Slow concentration of the filtrate yielded a dark brown, microcrystalline solid. Yield: 0.156 g (98%). Recrystallization from pentane yielded X-ray quality crystals. ^1H NMR (C_6D_6, 400.13 MHz): δ = 1.39 (s, 27 H, CH_3), 4.11 ppm (s, 5 H, Cp). $^{13}C\{^1H\}$ NMR (C_6D_6, 100.63 MHz): δ = 25.5 (*C*CH_3), 31.6 (CH_3), 86.2 (Cp), 215.1 ppm (CO). $^{29}Si\{^1H\}$ NMR (C_6D_6, 59.6 MHz): δ = 29.2 ppm. ^1H NMR (CD_2Cl_2, 300.0 MHz): δ = 1.13 (s, 27 H, CH_3), 5.02 ppm (s, 5 H, Cp). $^{13}C\{^1H\}$ NMR (CD_2Cl_2, 75.4 MHz): δ = 25.3 (*C*CH_3), 31.3 (CH_3), 86.9 (Cp), 215.1 ppm (CO). IR (hexane): $\tilde{\nu}$ = 2035 (s), 1988 (s) cm^{-1} (CO). IR (CH_2Cl_2): $\tilde{\nu}$ = 2030 (s), 1982 (s) cm^{-1} (CO). $C_{19}H_{32}FeO_2SSi$ (408.45): calcd. C 55.87, H 7.90; found C 54.59, H 7.85.

X-ray Structural Characterization: Data were collected with a Stoe IPDS-II two circle diffractometer with graphite-monochromated Mo-K_α radiation. Empirical absorption corrections were performed with the MULABS option[99] in the program PLATON.[100] Equivalent reflections were averaged. The structures were solved by direct methods[101] and refined with full-matrix least-squares on F^2 using the program SHELXL-97.[102] Hydrogen atoms were placed at ideal positions and refined with fixed isotropic displacement parameters using a riding model. Complex **17**: Two of the three *t*Bu substituents are disordered over two sites and were refined isotropically. In order to keep the geometric parameters in reasonable ranges, similarity restraints were applied for bond lengths and bond angles. Details of the X-ray crystal structure analyses of compounds **11I**, **12a**, **12b**, and **13** are summarized in Table 5 and compounds **15PF$_6$**, **16b**, and **17** in Table 6.

CCDC-628090 (**11I**), -628087 (**12a**), -628088 (**12b**), -628091 (**13**), -628094 (**15PF$_6$**), -628093 (**16b**), -628092 (**17**), and -628089 ([(18-crown-6)$(thf)_2$Na][4,4′-$(SitBu_2Me)_2(C_6H_4)_2$]) contain the supplementary crystallographic data for this paper. These data can be obtained free of charge from The Cambridge Crystallographic Data Center via www.ccdc.cam.ac.uk/data_request/cif.

Supporting Information (see footnote on the first page of this article): Calculated molecular structures of compounds **2b**, **2b**-H, **5b**, **5b**-H, **6b**, and **6b**-H (Figure S1).

Acknowledgments

The authors are grateful to the Deutsche Forschungsgemeinschaft (DFG) and the Fonds der Chemischen Industrie (FCI) for financial support and to Chemetall for the donation of *t*BuLi. We gratefully acknowledge computer time provided by the Frankfurt Center for Scientific Computing.

[1] C. A. Tolman, *Chem. Rev.* **1977**, *77*, 313–348.
[2] S. Trofimenko, *Scorpionates: The Coordination Chemistry of Polypyrazolylborate Ligands*, Imperial College Press, **1999**.
[3] B. Cornils, W. A. Herrmann, *Applied Homogeneous Catalysis with Organometallic Compounds*, Wiley-VCH, Weinheim, **1996**.
[4] A. Haghiri Ilkhechi, J. M. Mercero, I. Silanes, M. Bolte, M. Scheibitz, H.-W. Lerner, J. M. Ugalde, M. Wagner, *J. Am. Chem. Soc.* **2005**, *127*, 10656–10666.

[5] S. Bieller, M. Bolte, H.-W. Lerner, M. Wagner, *Chem. Eur. J.* **2006**, *12*, 4735–4742.
[6] S. Bieller, M. Bolte, H.-W. Lerner, M. Wagner, *Inorg. Chem.* **2005**, *44*, 9489–9496.
[7] S. Bieller, M. Bolte, H.-W. Lerner, M. Wagner, *J. Organomet. Chem.* **2005**, *690*, 1935–1946.
[8] A. Haghiri Ilkhechi, M. Bolte, H.-W. Lerner, M. Wagner, *J. Organomet. Chem.* **2005**, *690*, 1971–1977.
[9] S. Bieller, F. Zhang, M. Bolte, J. W. Bats, H.-W. Lerner, M. Wagner, *Organometallics* **2004**, *23*, 2107–2113.
[10] A. Haghiri Ilkhechi, S. Guo, M. Bolte, M. Wagner, *Dalton Trans.* **2003**, 2303–2307.
[11] T. I. Kückmann, M. Hermsen, M. Bolte, M. Wagner, H.-W. Lerner, *Inorg. Chem.* **2005**, *44*, 3449–3458.
[12] F. Dornhaus, M. Bolte, H.-W. Lerner, M. Wagner, *Eur. J. Inorg. Chem.* **2006**, 5138–5147.
[13] T. S. Lobana, in *Coordination Chemistry of Phosphane Chalcogenides and Their Analytical and Catalytic Applications*, *Vol. 2* (Ed.: F. R. Hartley), John Wiley & Sons, Chichester, **1992**, pp. 409–566.
[14] L. H. Gade, *Koordinationschemie*, Wiley-VCH, Weinheim, **1998**.
[15] T. D. Tilley, in *The Chemistry of Organic Silicon Compounds*, *Vol. 1* (Eds.: S. Patai and Z. Rappoport), John Wiley & Sons, New York, **1989**, pp. 1415–1477.
[16] J. Y. Corey, J. Braddock-Wilking, *Chem. Rev.* **1999**, *99*, 175–292.
[17] H. Nakazawa, K. Kamata, M. Itazaki, *Chem. Commun.* **2005**, 4004–4006.
[18] M. Okazaki, S. Ohshitanai, M. Iwata, H. Tobita, H. Ogino, *Coord. Chem. Rev.* **2002**, *226*, 167–178.
[19] R. D. Brost, G. C. Bruce, F. L. Joslin, S. R. Stobart, *Organometallics* **1997**, *16*, 5669–5680.
[20] D. L. Lichtenberger, A. Rai-Chaudhuri, *J. Am. Chem. Soc.* **1991**, *113*, 2923–2930.
[21] J. Chatt, C. Eaborn, S. Ibekwe, *Chem. Commun. (London)* **1966**, 700–701.
[22] H. Tobita, K. Hasegawa, J. J. G. Minglana, L.-S. Luh, M. Okazaki, H. Ogino, *Organometallics* **1999**, *18*, 2058–2060.
[23] J.-M. Camus, J. Andrieu, P. Richard, R. Poli, C. Darcel, S. Jugé, *Tetrahedron: Asymmetry* **2004**, *15*, 2061–2065.
[24] B. Wolfe, T. Livinghouse, *J. Am. Chem. Soc.* **1998**, *120*, 5116–5117.
[25] T. Miura, H. Yamada, S.-I. Kikuchi, T. Imamoto, *J. Org. Chem.* **2000**, *65*, 1877–1880.
[26] B. Wolfe, T. Livinghouse, *J. Org. Chem.* **2001**, *66*, 1514–1516.
[27] H. Dorn, C. A. Jaska, R. A. Singh, A. J. Lough, I. Manners, *Chem. Commun.* **2000**, 1041–1042.
[28] A.-C. Gaumont, M. B. Hursthouse, S. J. Coles, J. M. Brown, *Chem. Commun.* **1999**, 63–64.
[29] W. Angerer, W. S. Sheldrick, W. Malisch, *Chem. Ber.* **1985**, *118*, 1261–1266.
[30] D. A. Hoic, W. M. Davis, G. C. Fu, *J. Am. Chem. Soc.* **1996**, *118*, 8176–8177.
[31] V. V. Grushin, *Chem. Rev.* **2004**, *104*, 1629–1662.
[32] R. Weber, U. Englert, B. Ganter, W. Keim, M. Möthrath, *Chem. Commun.* **2000**, 1419–1420.
[33] C. Abu-Gnim, I. Amer, *J. Organomet. Chem.* **1996**, *516*, 235–243.
[34] B. Marciniec, H. Maciejewski, *Coord. Chem. Rev.* **2001**, *223*, 301–335.
[35] S. E. Denmark, J. D. Baird, *Chem. Eur. J.* **2006**, *12*, 4954–4963.
[36] P. T. Wolczanski, *Polyhedron* **1995**, *14*, 3335–3362.
[37] J. L. Bennett, P. T. Wolczanski, *J. Am. Chem. Soc.* **1994**, *116*, 2179–2180.
[38] K. F. Hirsekorn, A. S. Veige, M. P. Marshak, Y. Koldobskaya, P. T. Wolczanski, T. R. Cundari, E. B. Lobkovsky, *J. Am. Chem. Soc.* **2005**, *127*, 4809–4830.
[39] B. Marciniec, P. Krzyzanowski, E. Walczuk-Gusciora, W. Duczmal, *J. Mol. Catal. A* **1999**, *144*, 263–271.
[40] F. A. Cotton, C. S. Kraihanzel, *J. Am. Chem. Soc.* **1962**, *84*, 4432–4438.
[41] P. S. Braterman, D. W. Milne, E. W. Randall, E. Rosenberg, *J. Chem. Soc., Dalton Trans.* **1973**, 1027–1031.
[42] B. E. Mann, B. F. Taylor, *^{13}C NMR Data for Organometallic Compounds*, Academic Press, London, **1981**, p. 326.
[43] P. M. Treichel, D. A. Komar, *J. Organomet. Chem.* **1981**, *206*, 77–88.
[44] H. Schumann, L. Eguren, *J. Organomet. Chem.* **1991**, *403*, 183–193.
[45] E. E. Isaacs, W. A. G. Graham, *J. Organomet. Chem.* **1976**, *120*, 407–421.
[46] M. L. Brown, J. L. Cramer, J. A. Ferguson, T. J. Meyer, N. Winterton, *J. Am. Chem. Soc.* **1972**, *94*, 8707–8710.
[47] A. S. Goldman, D. R. Tyler, *Inorg. Chem.* **1987**, *26*, 253–258.
[48] E. Louattani, A. Lledós, J. Suades, *Organometallics* **1995**, *14*, 1053–1060.
[49] H. Schumann, *J. Organomet. Chem.* **1987**, *320*, 145–162.
[50] U. Schubert, G. Kraft, E. Walther, *Z. Anorg. Allg. Chem.* **1984**, *519*, 96–106.
[51] W. Malisch, H. Jehle, S. Möller, G. Thum, J. Reising, A. Gbureck, V. Nagel, C. Fickert, W. Kiefer, M. Nieger, *Eur. J. Inorg. Chem.* **1999**, 1597–1605.
[52] W. Malisch, H. Jehle, D. Schumacher, M. Binnewies, N. Söger, *J. Organomet. Chem.* **2003**, *667*, 35–41.
[53] J. S. McIndoe, B. K. Nicholson, *J. Organomet. Chem.* **2002**, *648*, 237–245.
[54] T. S. Piper, D. Lemal, G. Wilkinson, *Naturwissenschaften* **1956**, *43*, 129.
[55] W. Malisch, M. Kuhn, *Chem. Ber.* **1974**, *107*, 979–995.
[56] R. J. P. Corriu, W. E. Douglas, *J. Organomet. Chem.* **1973**, *51*, C3–C4.
[57] G. Cerveau, E. Colomer, R. Corriu, W. E. Douglas, *J. Organomet. Chem.* **1977**, *135*, 373–386.
[58] F. Dornhaus, M. Bolte, H.-W. Lerner, M. Wagner, *Eur. J. Inorg. Chem.* **2006**, 1777–1785.
[59] H. Nakazawa, Y. Ueda, K. Nakamura, K. Miyoshi, *Organometallics* **1997**, *16*, 1562–1566.
[60] N. Kuhn, H. Schumann, *J. Organomet. Chem.* **1986**, *304*, 181–193.
[61] M. Morán, I. Cuadrado, C. Pascual, J. R. Masaguer, J. Losada, *Inorg. Chim. Acta* **1987**, *132*, 257–262.
[62] I. Kovács, F. Bélanger-Gariépy, A. Shaver, *Inorg. Chem.* **2003**, *42*, 2988–2991.
[63] N. J. Coville, E. A. Darling, A. W. Hearn, P. Johnston, *J. Organomet. Chem.* **1987**, *328*, 375–385.
[64] F. W. G. Fearon, H. Gilman, *J. Organomet. Chem.* **1967**, *9*, 403–411.
[65] A. Sekiguchi, T. Fukawa, M. Nakamoto, V. Y. Lee, M. Ichinohe, *J. Am. Chem. Soc.* **2002**, *124*, 9865–9869.
[66] N. Wiberg, K. Amelunxen, H.-W. Lerner, H. Schuster, H. Nöth, I. Krossing, M. Schmidt-Amelunxen, T. Seifert, *J. Organomet. Chem.* **1997**, *542*, 1–18.
[67] Crystallographic data for [(18-crown-6)(thf)$_2$Na][4,4′-(Si*t*Bu$_2$Me)$_2$(C$_6$H$_4$)$_2$]: empirical formula $C_{58}H_{106}NaO_{10}Si_2$; formula mass 1042.60; green block; T = 173(2) K, crystal system monoclinic; space group $P2_1/c$; unit cell dimensions a = 13.1292(8), b = 18.3379(8), c = 14.4381(8) Å, β = 113.233(4)°; V = 3194.3(3) Å^3; Z = 2; $D_{calcd.}$ = 1.084 g cm^{-3}; μ = 0.112 mm^{-1}; $F(000)$ = 1146; crystal size 0.40 × 0.23 × 0.22 mm; reflections collected = 40036; independent reflections = 5846 [R(int)= 0.0665]; data/restraints/parameters = 5846/12/318; GOOF on F^2 = 1.086; final R [$I > 2\sigma(I)$]: R_1 = 0.0999, wR_2 = 0.2692; R (all data): R_1 = 0.1169, wR_2 = 0.2834; largest diff. peak and hole 0.716 and –0.528 e Å^{-3}. The solvent thf molecule is disordered over two positions and was refined isotropically. In order to keep the geometric parameters in reasonable ranges, bond length restraints of C–O = 1.40(1) and C–C = 1.50(1) Å as well as restraints of 2.5(1) Å for 1,3-distances were applied.

[68] T. H. Whitesides, J. Shelly, *J. Organomet. Chem.* **1975**, *92*, 215–226.
[69] S. B. Fergusson, L. J. Sanderson, T. A. Shackleton, M. C. Baird, *Inorg. Chim. Acta* **1984**, *83*, L45–L47.
[70] M. L. H. Green, C. N. Street, G. Wilkinson, *Z. Naturforsch., Teil B* **1959**, *14*, 738.
[71] A. F. Holleman, N. Wiberg, *Lehrbuch der Anorganischen Chemie*, Walter de Gruyter, Berlin, **1995**, p. 2033.
[72] It appears that rather than attacking the iron atom, the nucleophilic siloxide reacts with the iodide ligand to form an $[Fp]^-$ fragment and intermediate $IOSiPh_2Me$. The complex iron anion subsequently reacts with one equivalent of FpI to give Fp_2. We speculate that the intermediate silicon-containing species reacts with one equivalent of siloxide ligand to give disiloxane $O(SiPh_2Me)_2$ and NaIO. The disiloxane is also the major product when **Na7** is treated with I_2. This can be thought of as analogous to the reaction of I_2 with OH^-, which results in IO_3^-, I^-, and H_2O.[71] When the same reaction is carried out using FpBr rather than FpI, an identical outcome is observed. However, the formation of Fp_2 and $O(SiPh_2Me)_2$ from **Na7** and FpI is slow, with about 50% of the starting material left after stirring for two weeks at room temperature. This slow reaction rate allows for the isolation of an adduct of **Na7** and Fp_2 in which the siloxide sodium atoms are supported by donor–acceptor interactions with the oxygen atoms of the bridging carbonyl ligands in Fp_2. The details of this adduct formation have been discussed recently in another context.[73]
[73] T. I. Kückmann, M. Bolte, H.-W. Lerner, M. Wagner, *Z. Anorg. Allg. Chem.* **2007**, *633*, 290–297.
[74] F. H. Allen, *Acta Crystallogr., Sect. B* **2002**, *58*, 380–388) (Cambridge Crystallographic Database, CSD Version 5.27, November 2005; update August 2006).
[75] L. Párkányi, K. H. Pannell, C. Hernandez, *J. Organomet. Chem.* **1983**, *252*, 127–132.
[76] R. West, E. K. Pham, *J. Organomet. Chem.* **1991**, *402*, 215–220.
[77] N. Kuhn, H. Schumann, *J. Organomet. Chem.* **1984**, *276*, 55–66.
[78] L. D. Quin, *A Guide to Organophosphorus Chemistry*, John Wiley and Sons, Inc., New York, **2000**, p. 394.
[79] S. Berger, S. Braun, H.-O. Kalinowski, *^{31}P-NMR-Spektroskopie*, Thieme Verlag, Stuttgart, **1993**.
[80] H. A. Bent, *Chem. Rev.* **1961**, *61*, 275–311.
[81] P. M. Treichel, W. K. Dean, W. M. Douglas, *J. Organomet. Chem.* **1972**, *42*, 145–158.
[82] M. Green, D. J. Westlake, *J. Chem. Soc. A.* **1971**, 367–371.
[83] P. M. Treichel, R. L. Shubkin, K. W. Barnett, D. Reichard, *Inorg. Chem.* **1966**, *5*, 1177–1181.
[84] A. Schäfer, H. Horn, R. Ahlrichs, *J. Chem. Phys.* **1992**, *97*, 2571–2577.
[85] A comparison of the averaged computed harmonic CO stretching frequencies [obtained as $(\tilde{\nu}_{as} + \tilde{\nu}_s)/2$] with the averaged experimentally determined frequencies revealed a systematic deviation. A scaling factor of 0.9884 was therefore employed to improve the overall agreement.
[86] W. Koch, M. C. Holthausen, *A Chemist's Guide to Density Functional Theory*, Wiley-VCH, Weinheim, **2001**.
[87] A. Schäfer, C. Huber, R. Ahlrichs, *J. Chem. Phys.* **1994**, *100*, 5829–5835.
[88] M. J. Frisch, G. W. Trucks, H. B. Schlegel, G. E. Scuseria, M. A. Robb, J. R. Cheeseman, J. J. A. Montgomery, T. Vreven, K. N. Kudin, J. C. Burant, J. M. Millam, S. S. Iyengar, J. Tomasi, V. Barone, B. Mennucci, M. Cossi, G. Scalmani, N. Rega, G. A. Petersson, H. Nakatsuji, M. Hada, M. Ehara, K. Toyota, R. Fukuda, J. Hasegawa, M. Ishida, T. Nakajima, Y. Honda, O. Kitao, H. Nakai, M. Klene, X. Li, J. E. Knox, H. P. Hratchian, J. B. Cross, C. Adamo, J. Jaramillo, R. Gomperts, R. E. Stratmann, O. Yazyev, A. J. Austin, R. Cammi, C. Pomelli, J. W. Ochterski, P. Y. Ayala, K. Morokuma, G. A. Voth, P. Salvador, J. J. Dannenberg, V. G. Zakrzewski, S. Dapprich, A. D. Daniels, M. C. Strain, O. Farkas, D. K. Malick, A. D. Rabuck, K. Raghavachari, J. B. Foresman, J. V. Ortiz, Q. Cui, A. G. Baboul, S. Clifford, J. Cioslowski, B. B. Stefanov, G. Liu, A. Liashenko, P. Piskorz, I. Komaromi, R. L. Martin, D. J. Fox, T. Keith, M. A. Al-Laham, C. Y. Peng, A. Nanayakkara, M. Challacombe, P. M. W. Gill, B. Johnson, W. Chen, M. W. Wong, C. Gonzalez, J. A. Pople, *Gaussian 03, Revision B.3*, Gaussian, Inc., Pittsburgh, PA, **2003**.
[89] *Spartan 06.1*, Wavefunction, Inc., Irvine, CA, **2006**.
[90] It is reasonable to assume that the final products of hydride abstraction for both the oxide **5b** and the phosphanyl borohydride **2b** will be cyclic dimers or polymers of the corresponding boranes. Nonetheless, the first intermediates following hydride abstractions are key species along the reaction pathways, and these are likely to be as described above.
[91] H. E. Gottlieb, V. Kotlyar, A. Nudelman, *J. Org. Chem.* **1997**, *62*, 7512–7515.
[92] V. D. Bianco, S. Doronzo, *Inorg. Synth.* **1976**, *16*, 161–163.
[93] G. Stieglitz, B. Neumüller, K. Dehnicke, *Z. Naturforsch. Teil B* **1993**, *48*, 156–160.
[94] T. J. Barton, C. R. Tully, *J. Org. Chem.* **1978**, *43*, 3649–3653.
[95] N. Wiberg, C.-K. Kim, *Chem. Ber.* **1986**, *119*, 2980–2994.
[96] T. Ohishi, Y. Shiotani, M. Yamashita, *J. Org. Chem.* **1994**, *59*, 250.
[97] D. Catheline, D. Astruc, *Organometallics* **1984**, *3*, 1094–1100.
[98] D. L. Reger, C. Coleman, *J. Organomet. Chem.* **1977**, *131*, 153–162.
[99] R. H. Blessing, *Acta Crystallogr., Sect. A* **1995**, *51*, 33–38.
[100] A. L. Spek, *Acta Crystallogr., Sect. A* **1990**, *46*, C34.
[101] G. M. Sheldrick, *Acta Crystallogr., Sect. A* **1990**, *46*, 467–473.
[102] G. M. Sheldrick, *SHELXL-97, A Program for the Refinement of Crystal Structures*, Universität Göttingen, Germany, **1997**.

Received: November 21, 2006
Published Online: April 4, 2007

